CODEN:LUTMDN/(TMMV-5304)/1-38/2020

LUND
UNIVERSITY

Chemical Vapor Deposition of Titanium Oxycarbide

Carl Henrik Dahmén
tfy15cda@student.lu.se

A thesis presented for the degree of
Master of Science

June 25, 2020

Seco Tools AB & The Department of Production and Materials Engineering
Lund University, Faculty of Engineering, LTH

Supervisor: Filip Lenrick filip.lenrick@iprod.lth.se
Examiner: Jan-Eric Ståhl jan-eric.stahl@lth.lu.se

Abstract

Ti(C,O) coatings have been generated in a hot wall CVD system on WC/Co, fine and coarse grained Ti(C,N), TiN, Cr and c-BN substrates. The research in this thesis has focused on deposition, characterization, and analysis in the perspective of the bonding layer of a coated insert. The precursors, H_2, $TiCl_4$, CO, temperature and pressure have been coupled to the texture using a Design of Experiment software. Samples have been characterized by XRD, SEM and TEM prepared by FIB. Analysis of crystal growth is based on a literature study of Ti(C,N), TiN, TiC and CO adsorption on transition metals. Rare up to 10μm long "five-ling" multiple twinned crystals have been obtained at a pressure of 0.5 atm and 1000°C. Favorable crystal growth on the Ti(C,N) substrate in the perspective of a bonding layer in a cutting tool insert was found for 1000°C, $TiCl_4/CO \geq 1$ in a H_2 rich environment. The lattice parameter at different deposition conditions varied from 4.270 to 4.295 Å. Ti(C,O) coatings demonstrate thin, high index grains centered around the (111) twinning boundary, the literature analysis of CO adsorption indicates these are made possible due to the adsorption properties of CO.

Keywords: CVD, Hard Coatings, Ti(C,O), CO, Five-ling twinned crystals.

Contents

1 Introduction

The history of Sweden is a history of iron, beginning way back when the vikings forged their hammers and swords for their raids in Europe. In Bergslagen iron have been commercially exported since the fourteenth century and united us with the rest of Europe. Gustav Vasa nationalized and effectivized the ironworks and fortified Sweden as a nation. 1611 the first ironwork was established in what is now Fagersta. During the nineteenth century with the entry of industrialization, the market became competitive and the Swedish steel industry had to innovative. Fagersta Bruk aktiebolag was founded 1873 and was one of the most significant ironworks in Sweden, their work was exhibited on the 1900 Paris Exposition. During the thirties Fagersta Bruk diversified its assortment with the slogan "Ett stål för varje ändamål", (a steel for every use). This turned out to be a smart move and their excellent tungsten carbide that Seco Tools owns it success to, had its origin from this time. After WW2 Swedish steel and Fagersta bruk had their prime time that lasted all the way until the steel crisis in the early seventies. A crisis much due to the globalization and cheaper steel produced in Soviet and China. Once again the Swedish steel industry had to innovate and Seco Tools was born and would now create tools for cutting the same steel that put Fagersta Bruk out of business. Today the market is more competitive than ever, in the last twenty years the annual car production has almost doubled, 90 million cars which all need their sheet metal cut. To keep up with the demand the cutting speed have to constantly increase and this is where the cutting tool insert is the main character.[1]

Figure 1 Turning tool insert from Seco Tools [2].

1.1 *Cutting Edge Technology*

A cutting tool insert for cutting or a turning tool for turning (see Figure 1) is a separable piece consisting of a cutting edge by a multilayer of coatings on a piece of cemented carbide body made of WC (tungsten carbide) and cobalt. The insert is attached to the cutting tool body and can be exchanged after the edge is worn or for change of function. By producing a small insert with extreme qualities, the rest of the machine tool can be made of a less-expensive tougher material. This have substantially increased the cutting speed and insert based tools are by now in wide spread use.
A modern insert for high speed processing needs extreme properties to machine steels and super alloys. At temperatures of about 1000°C and pressures of about 1-2 GPa, the inserts have to be resilient to wear and mechanical impacts to assure an acceptable life time and a high cutting speed.
The coating on inserts usually consists of several different layers with intermediate bonding layers. Typically the layers are deposited by Chemical Vapor Deposition (*CVD*). Aluminum oxide (Al_2O_3) is a common top layer, for its a good abrasiveness and high heat conductivity and will protect the underlying layer from oxidization. Titanium carbonitride (*Ti(C,N)*) has been widely used as an underlying layer for its high melting point, hardness, chemical stability, and low friction. The deposition conditions have been optimized for performance and the engineers have a fine control of the microstructure, adhesion and thickness etc. However, as far as of today flaking of the aluminum oxide layer due to an insufficient bonding layer restricts the cutting speed. A promising candidate for an additional or alternative layer, is a similar compound to Ti(C,N). Namely titanium oxycarbide (*Ti(C,O)*). Ti(C,O) is rather unexplored and the literature this thesis is based on, is of similar compounds. The goal of this thesis is to create a process space to correlate parameters to change of morphology in the perspective of a bonding layer.

2 Chemical Vapor Deposition (CVD)

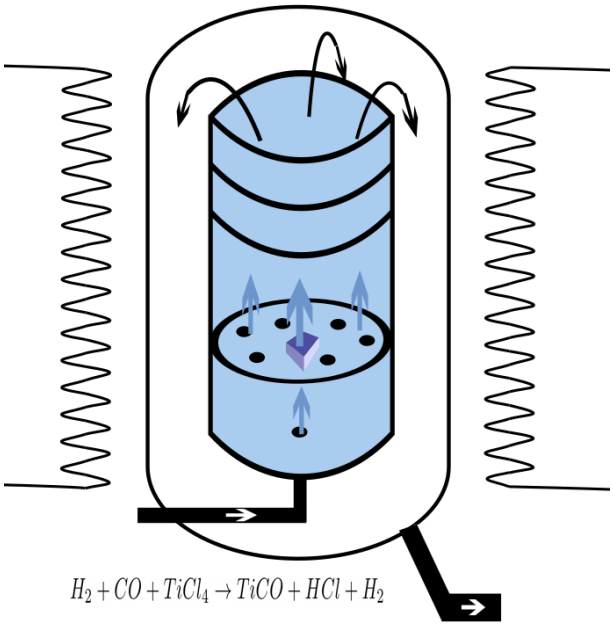

Figure 2 Schematic view of the hot wall CVD system at Seco Tools.

2.1 Hot wall CVD

Chemical vapor deposition is a method used to produce high quality coatings with the goal of creating well adhering coatings with desired properties. At Seco Tools a hot wall CVD is used both on the research and production line where 10 000 inserts are coated at a time. Compared to *physical vapor deposition* (PVD) the other deposition technique in use at Seco Tools, enables CVD a wide range of materials in uniform thick or thin coatings and on different topographies. The CVD process begins with injection of the gas precursors to the reactor chamber (see Figure 2) from connected tanks regulated by mass flow gauges. The insert is positioned on a crucible and placed in the temperature and pressure controlled reaction chamber. The reactants will flow around and expose the inserts and on the surfaces deposit solid material through chemical reactions. A constant flow in the chamber is imposed for a homogeneous atmosphere and in order to get rid of reaction products.

2.2 Deposition rate control

There are many factors at play in the design of a CVD experiment and the process steps and reaction mechanisms can be complicated and very few are known. Variable parameters to control the synthesis are temperature, pressure and precursors.
Temperature is usually an important parameter for controlling deposition rates. The Arrhenius equation (Equation 1) describes the deposition rate as a function of activation energy E_a. The activation energy is the energy which must be provided to activate a certain process. By studying the activation energy as a function of temperature it is possible to discern the dominating process for the given instance. [3].

$$k_m = A \cdot e^{\frac{-E_a}{k_B T}} \tag{1}$$

k_m is the deposition rate, A is a constant depending on the rate of collisions between the molecules, k_B is the Boltzmann constant and T is the temperature in Kelvin. By plotting the natural logarithm of the reaction rate as a function of the reciprocal temperature it is possible to characterize a few processes controlled mechanisms:

The *Surface kinetics controlled regime*, where fast diffusion rate and slow surface reactions take place, ensuring the atoms to diffuse to the energetically most favorable spots creating smooth and uniform surfaces.

In *Mass transport control*, a large concentration gradient towards the surface will form a fast deposition due to fast surface reactions and the mass transport in the vapor is slow.

When the process is under *Nucleation control* often at supersaturation, the nucleation of precursors can be slow and be the rate limiting mechanism.

At high temperatures and low flows the deposition rate will be proportional to the mass input rate and the process will be governed by pressure and temperature, which is characteristic of *Thermodynamic control*.

All surface reactions, diffusion and deposition will occur at a thin layer above the surface with a laminar flow, (the boundary layer) and will have a big effect on the morphology. The thickness of the boundary layer δ and the diffusion coefficient D controls the *reaction resistance* : [4]

$$\frac{\delta}{D} = c \cdot \frac{P^{1/2}}{T^{1.75-m/2}} \tag{2}$$

c is an unitless constant; m a constant of $(0.6 \leq m \leq 1.0)$; P the total pressure and T the temperature.
The reaction resistance will thus decrease the reaction rate at higher temperature and

pressure, though this will be countered by the increase in growth rate described by the Arrhenius equation which is more rapid.

3 Crystal Structure and Synthesis

3.1 Similar compounds to Ti(C,O)

Ti(C,O) is not very well described in the literature. Its sister compounds Ti(C,N), TiN and TiC possess a larger knowledge base. Ti(C,O) is similar to these compounds, belonging to the same crystal lattice group and having similar chemical properties, the difference lay mostly in surface, boundary and strain energies. But these are the main sources to crystal growth mechanisms. In TiN and Ti(C,N) the correlation between certain texture and morphology have been mapped to process parameters. If Ti(C,O) exhibits similar structures their results can be extrapolated and the differences will be due to said energies.

3.1.1 Ti(C,N)

Ti(C,N) is in wide use at Seco Tools and has thus been studied in detail. In Figure 3 an example of Ti(C,N) growth is demonstrated. The surface in 3b is one of the substrates used in the experiments, a favorable Ti(C,O) growth on this surface is of high interest.

(a) Schematic cross section of a Ti(C,N)(<211>) grain.

(b) Top view of <211> oriented Ti(C,N) grains and twinning planes indicated by dashed white lines.

Figure 3 Coarse grained Ti(C,N). From Ref. [5].

In Figure 3, a Ti(C,N)(<211>) grain is depicted. The <211> plane is parallel to the surface growing in the [111] direction, the sides of the grain are (100) planes. The white balls in 3a are titanium and black is carbon or nitrogen. The <211> grain grow by atoms being adsorbed to the {111} growth plane on the surface, resulting in the grains seen in Figure 3b.

3.2 Synthesis

Titanium Oxycarbide was obtained using the CVD system in Figure 2. After the desired temperature and pressure is reached the precursor gases, $TiCl_4$, CO and H_2 are injected into the reactor chamber and the chemical reaction leading to Ti(C,O) growth expressed as following, could take place.

$$TiCl_4(g) + CO(g) + 2H_2(g) \rightarrow TiCO(s) + 4HCl(g) \tag{3}$$

The nature of CO makes it only possible to release equal parts of Carbon and Oxygen, a relation that is not necessarily retained in the solid Ti(C,O) and can range from 100 % TiC to 100 % TiO.

The reaction will occur in different steps depending on the process regime and location but for $TiCl_4$ to react with CO, H_2 is used as a transport gas as well for forming HCl, see Reaction 4.

$$TiCl_4 + 2H_2 \rightarrow Ti + 4HCl \tag{4}$$

3.2.1 CO adsorption

The Ti(C,O) synthesis is mainly a heterogeneous catalysis, the reaction occur on and with the surface. Adsorption of CO on the transition metals have been studied by R. R. Ford [6]. The carbon atom have a small negative charge compared to the oxygen atom thus carbon monoxide inhibits a small dipole moment. Ti is a transition metal, meaning it has a partially filled d-sub shell, where CO will bond to. Because of this carbon monoxide is foremost adsorbed with the carbon atom to the surface, see Figure 4. A process depending on the relative availability of bonds. The donor ability of CO is known to be small and the bonding to the metal is therefore most likely to adsorb to hollow sites or between positive ions, see Figure 4c. For reactive transition metals like titanium the chemisorption is primarily of an dissociative process; the carbon monoxide molecule is adsorbed and will then loose the oxygen which in its turn will diffuse and form the oxycarbide. While in molecular adsorption the carbon and oxygen bond will retain. Both these two types can exist simultaneously and is very sensitive to the activation energy due to surface temperature and crystal orientation. [6]

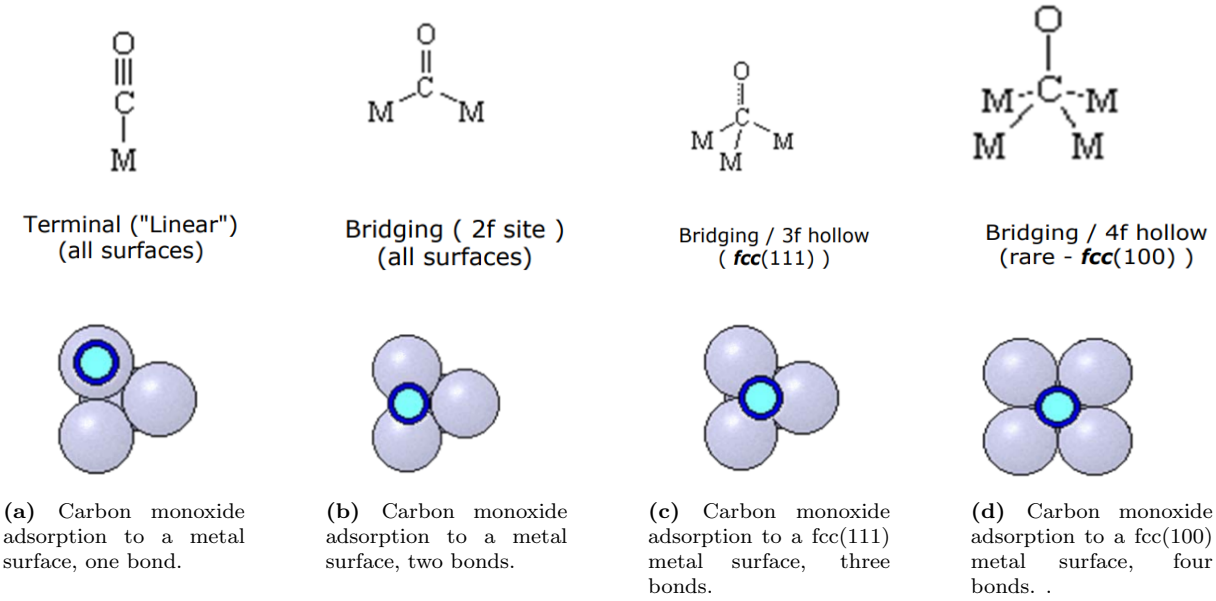

(a) Carbon monoxide adsorption to a metal surface, one bond.

(b) Carbon monoxide adsorption to a metal surface, two bonds.

(c) Carbon monoxide adsorption to a fcc(111) metal surface, three bonds.

(d) Carbon monoxide adsorption to a fcc(100) metal surface, four bonds. .

Figure 4 4 kinds of CO bonding to a pure metal surface. Violet balls illustrate the metal atom, dark blue carbon and light blue oxygen. Figure from Ref. [7].

In Figure 4 molecular adsorption of the carbon monoxide molecule to a metal surface is displayed, for dissociation of oxygen, the C-O bond also has to be broken. In Figure 4d two of the metal ions on Ti(C,O) would be C/O resulting in different kind of bonds. Influence of already adsorbed C and O will make the picture more complex. The chemisorption of carbon and oxygen is highly dependent on the orientation of the surface. In adsorption of carbon and nitrogen in Ti(C,N) the HCN molecule will adsorb at (100) surfaces and ensure a rapid braking of the triple bond [5]. Ruppi et al [8] describes the influence of CO under a varying partial pressure during Ti(C,N) synthesis. The composition study show the carbon composition to be constant while oxygen will increase on the behalf of and

superseding of initial nitrogen levels, while never surpassing carbon. This supports the hypothesis of adsorption of carbon being the primary reaction and adsorption of oxygen being the secondary.

3.3 Crystal structure

3.3.1 The unit cell

Ti(C,O) belongs to the sodium chloride crystal structure common among many ceramics. NaCl is mainly an ionic compound with strong forces between the positive and negative ions structured in a face-centered-cubic (FCC) lattice type, see Figure 5. In titanium compounds it is more complicated and the bonding structure consists of a combination of ionic, covalent, and metallic contributions [9]. NaCl structure is easiest thought of as layers of checkboards with altering colors in the direction of height where the different colors represent positive and negative ions. Ti(C,O) consists of Ti^+ ions represented by green balls and C^- or O^- ions represented by red in Figure 5.

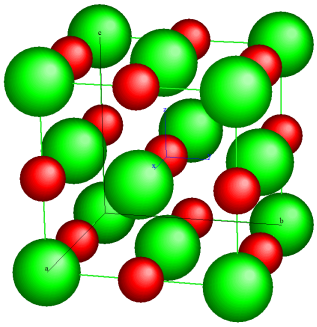

Figure 5 The face-centered cubic unit cell of the NaCl structure type.

An unit cell is defined as the smallest repeating unit in a crystal structure and for the cubic structures all axes are of equal length and orthogonal to each other. This axis or lattice parameter is usually denoted **a**. The length of the a axis is usually dependent on the chemical composition, in this case the ratio and total amount of non-metallic elements to the metallic element. Thus the C to O ratio and the C+O/Ti ratio in case of vacancies. Assuming a linear relation, the lattice parameter of Ti(C_x,O_{1-x}) can be calculated from TiC and TiO called Vegard's law [10]:

$$a = (1 - x)a_{TiO} + xa_{TiC} \tag{5}$$

The lattice parameter of TiO is 4.18 Å and of TiC 4.33 Å and the Ti(C,O) lattice parameter could theoretically vary between these two.

3.3.2 Vacancies

Vacancies are known to have a large effect on the electronic and structural properties of crystals. During the solidification of a material vacancies will increase exponentially with temperature, and often create a vacancy gradient at the surface. Depending on the cooling the concentration of vacancies are in a various degree retained, why annealing is often used to get rid of impurities, like vacancies.[11]

3.3.3 Crystal planes

If rock salt have a cubic structure why are the macroscopic salt crystal not cubic? In crystals there are geometric lines or planes linking the atoms together denoted (h,k,l), see Figure 6. These directions will have different density of atoms and other element distributions that influence the crystal behavior. Physical adsorption and reactivity occurs near surface atoms creating a growth preference for higher density planes. Planes will influence a range of properties of the crystal such as surface tension, refractive index, cleavage and deformation. In the case of a bonding layer the "bonding" is the sought after property and are realized by plenty nucleation sites and crystal plane spacings that line up with the material above.

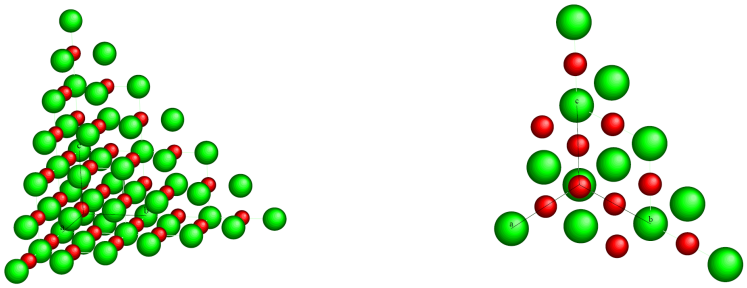

(a) (111)-plane **(b)** (211)-plane

Figure 6 A (111) and a (211) plane of the NaCl structure type.

For the cubic crystal structures the (hkl) planes are easiest imagined by considering their normal in the [hkl] direction. Notice how the (111) plane is consisting of one type of ion. If these planes are stacked in parallel to the substrate, X-ray diffraction will be able the discern the relative presence of the planes by discerning the plane's characteristic parallel distance, see Figure 11. Planes are constantly repeated in the crystal thus the (-2,1,1) plane will be the same as (2,1,1) and (2,-1,-1) etc. and all combinations there of.

3.3.4 Crystal surfaces

In order to calculate preferable growth orientations and surface energies, there are methods for performing electronic structure calculations for crystals with varying simplifications of the complex reality. These methods use what is called pseudopotentials, in replacement of the Coulombic potential of every electron in an atom to be then used in the Schrödinger equation. These models have shown to be very accurate and are often used in combination with experiments. But as soon as a surface is concerned the symmetry is broken and a full characterization requires that the composition of every layer is studied. A simple model of calculating surface energy is by counting broken chemical bonds. If that applies to Ti(C,O) the surface energy for (111) is expected to be the largest. This model is most accurate for pure ionic materials and studies of TiC have shown stable (111) titanium surfaces indicating covalent bonds [12]. Crystal surfaces do not have to be homogeneous, there is often a vacancy gradient and it can consist of altering facets and making surface energy calculations very complex. Planes will grow orderly and have certain angles between them, thus an unidentified plane growing with a certain angle onto a known plane, a measured angle could theoretically characterize the new plane. In the cubic system these angles can be calculated using linear algebra, for example will the (211) plane be orthogonal to the (111) plane, see equation 6.

$$(1,1,1) \times (-2,1,1) = -2 + 1 + 1 = 0 \tag{6}$$

Plane angles are calculated by scalar product:

$$\mathbf{a} \cdot \mathbf{b} = ||\mathbf{a}|| \, ||\mathbf{b}|| cos(\theta) \tag{7}$$

3.3.5 Crystal formation

(hkl) planes are not enough to explain the macroscopic shape of crystals, formations that can be rather complex. For a metallurgist crystals with well-developed faces are a secondary characteristic and thought most of as grains seen among others in a microscope. But in solid state physics and the semiconductor industry one-faceted crystals are directly linked to the performance of their technology.
Nature always strive after energy optimization and one have to take into account boundary energy, surface energy and elastic strain energy to mention a few, in the creation of crystals as seen at the macroscopic scale. Nature's way of self assembly is a very hot research area in all fields of nanotechnology, controlling it is a source of great potential.

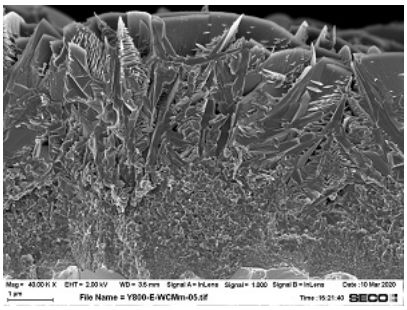

(a) Sample E on WC/Co, example of "evolutionary growth".

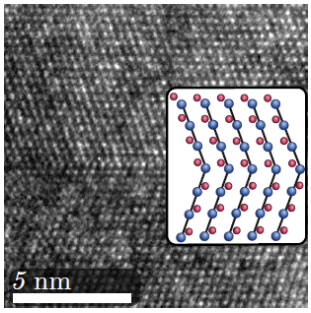

(b) Twin boundary [13] used by permission of author.

Figure 7 Example of *evolutionary growth* and the *twin boundary*.

3.3.6 Epitaxial growth

As crystal layers are formed they will grow with respect to the layer below. Are the interplanar spacings of the substrate and coating matching, similar crystal structure can be continued without strain. Minimization of the surface energy occur if atoms are adsorbed at steps and kinks rather than at a plane surface, thus are adsorption inclined to occur at ledges thus growing uniform layers, if in the surface kinetics controlled regime. Dislocations can be reinforced by the adsorption at the kinks they expose due to "permanental steps"[14]. Boundaries of substrate and coating are a source of strain and an unit cell mismatch are compensated by lateral strain. If the crystal orientation can not directly be translated the *evolutionary selection model* proposed by Van der Drift will take place, [9] consisting of the *nucleation stage* and *growth stage*. Various crystals will grow in the nucleation stage but due to the higher growth rate of some crystals and favorable growth directions they will "win" and all other orientations will be overshadowed in the growth stage, see an example in Figure 7a. Lowest energy surfaces will generally dominate the growth in NaCl type structure but due to the complicated bonding structure of titanium compounds, the surface energies of various faces are not well known [9].

3.3.7 Twinning planes

When two grains meet, the coinciding lattice is a region of relatively high energy. *Twinned planes* however have a lower energy and occur when two grains of different orientation share the same crystal lattice points in a symmetrical manner, see Figure 7b.[15].

3.3.8 Five-ling twinned crystal or *stars*

Star-shaped crystals have been obtained by CVD, in both TiN [16] and TiCN [17]. These stars are described to nucleate from nano sized decahedral particles constructed by five tetrahedra sharing the middle $\langle 110 \rangle$ axis and $\{111\}$ planes, frequently found in the early stages of nucleation of fcc metals and diamonds with a size in the tens of nanometers. See Figure 8.

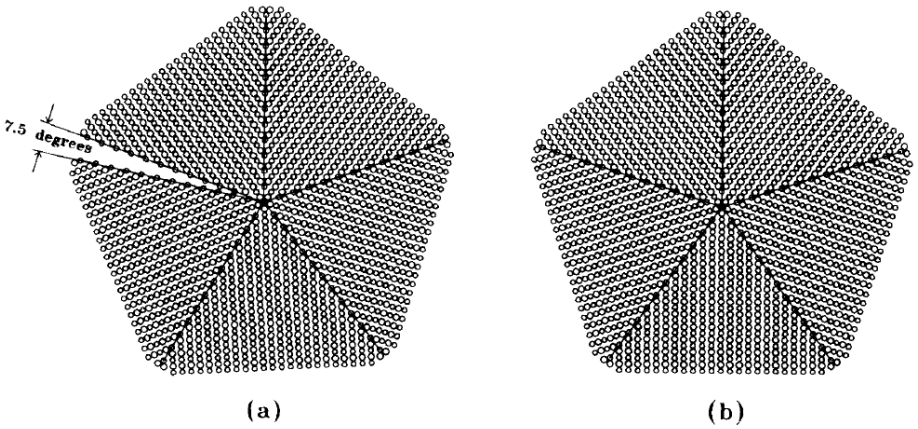

Figure 8 Decahedral particle, structure model for star-shaped nucleus. (a) Packing of five tetrahedra by sharing (110) axis without strain. (b) The 7.5° mismatch is released by elastic deformation of the five tetrahedra. Picture from "Growth mechanism of star-shaped TiN crystals" [16] used by permission of author.

There is an inherent mismatch of 7.5° for the decahedral preventing continued growth because of the increasing strain for larger structures of noble-metal nanocrystals described by Zhou et al [18]. At TiN and TiCN growth, Sun et al propose that the strain energy is released by growing tetrahedral arms sharing a twin boundary in the (111) plane as the five arms in the stars, see Figure 9 . These stars are described to have a quick growth, due to their extreme height and kinks on their surfaces. This process is related to *dendritic growth*. As the nucleation is poor and some type of saturation exist, a small solid protuberance or a *dendrite* will encourage growth, similar to undercooled water which requires a nucleation point to freeze. Like the reinforced dislocation, the twin intersection is a source of "permanent steps" thus providing an rapid growth rate [14].

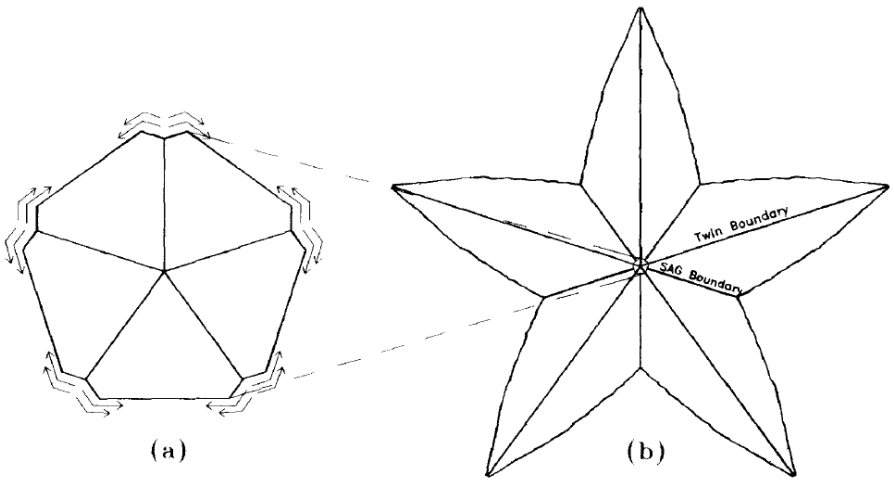

Figure 9 Growth model for star-shaped crystal. (a) Growth feature on the multiply-twinned nucleus (b) Schematic representation of the star-shaped crystal after growth. SAG abbreviation for small angle grain. Picture from "Growth mechanism of star-shaped TiN crystals" [16] used by permission of author.

4 Coating characterization

4.1 X-Ray Diffraction (XRD)

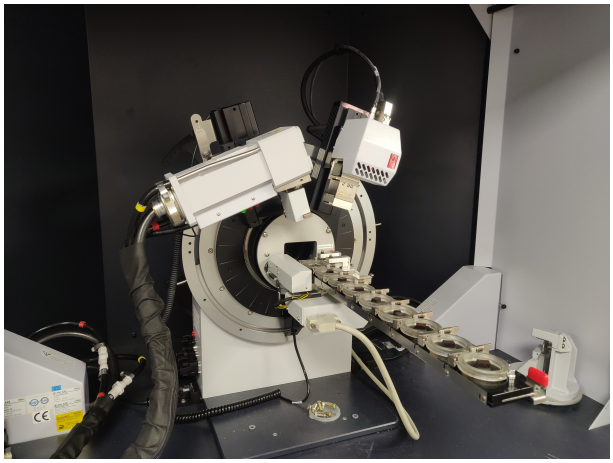

Figure 10 Bruker AXS diffractometer, with 9 sample holders.

X-ray diffraction is a tool for deciding the crystallographic phase composition of matter. X-rays are electromagnetic waves with wavelengths of 1-2 Å, in the same order as the atom radius. The incident beam will diffract from a set of parallel lattice planes in the crystal. By the different distances traveled by the reflected X-Rays, constructive interference will occur for specific angles making it possible to decide the plane spacing. Bragg's equation determines this according to:

$$2d_{hkl}sin\theta = \lambda \tag{8}$$

d_{hkl} is the interplanar spacing, λ the wave length and θ the angle of the incident beam see Figure 11.

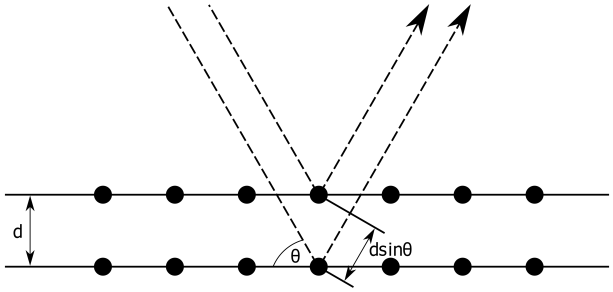

Figure 11 Schematic picture of atomic planes diffracting x-rays. [19]

The intensity of the diffracted rays are plotted as a function of the incident angles in a diffractogram giving the characteristic peaks of crystal phases. Each sample consists of a collection of crystal planes with their own characteristic diffractogram, comparing this to a reference data base provides the present crystal facets. A common texture characterizing coefficient using the Harris method [9] is the texture coefficient TC(hkl) defined as:

$$TC_{h_ik_il_i} = \frac{I(h_ik_il_i)/I_{ref}(h_ik_il_i)}{(1/n)\sum_{j=1}^{n}\frac{I(h_jk_jl_j)}{I_{ref}(I(h_jk_jl_j)}} \tag{9}$$

The TC(hkl) value is an indication of the volume-average of hkl planes oriented parallel to the sample surface in relation to all other planes. If the TC for all planes are 1, it is a random distribution of planes and a larger value indicates a larger occurrence.

The intensities has to be adjusted for thickness of the coating because rays with high incident angles (small θ) will travel in less material and thus lose intensity compared to orientations found at a lower θ. In this thesis the investigation of crystal planes was executed by a Bruker AXS diffractometer, see Figure 10.[20]

4.2 Scanning Electron Microscope (SEM)

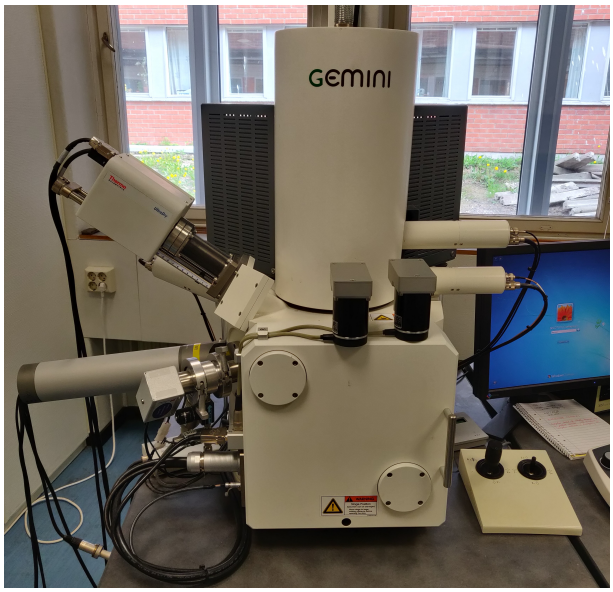

Figure 12 ZEISS ULTRA 55 - SEM at Seco Tools.

The resolution of optical microscopy is restricted by the wavelength of visible light. By the use of higher energy electrons it is possible to resolve features down to a couple of nanometers. The SEM generates an electron beam from an electron source in this case a thermal field emission type from the ZEISS ULTRA 55-SEM, see Figure 12. The electrons are then accelerated to 1-20 keV and focused by lenses and apertures before striking the sample. In the interaction with the surface different kinds of electron scattering impacts occurs, see Figure 13. The SEM is equipped with Secondary Electron (*SE*), Back-Scattered Electrons (*BSE*) and Energy Dispersive X-Ray (*EDX*) detectors. SE are produced by inelastic collisions with the valence electrons of the surface atoms resulting in ejected electrons with an energy of 50 eV and less. These are localized to the point of impact of the primary electron because of their low mean free path in solid material and generated from the surface down to a few nanometers. This makes it possible to resolve very small features on the nanometer-scale. A black and white picture from the intensities from the scattered electrons will be produced, due to more scattering surface edges and slopes tend to be brighter resulting in a high-contrast three-dimensional image.

BSE are produced by elastic collisions with atom nucleus and have a much larger energy than SE and will have a larger interaction volume and can travel deeper into the sample. The electrons will "backscatter" from the surface to the detector. More electrons will collide with atoms with larger atomic number Z, thus there is a material dependency on the intensity. Heavier materials will appear brighter than materials with a smaller atomic number.

EDX analysis is used to determine the elemental abundance and distribution. When a primary electron collides with a core shell electron it can be ejected thus creating a vacancy. Energy relaxation of the created ion occur as an outer electron fill the vacancy

emitting X-Rays in the process. These X-Rays, as their intensity are characteristic for different materials making chemical analysis possible.

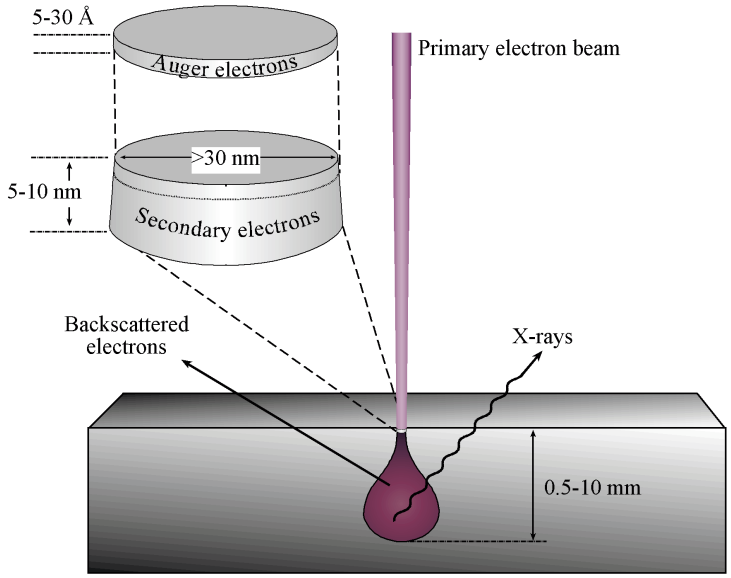

Figure 13 The activated volume and escape depths for the detected electrons and radiation. [4]

4.3 Transmission Electron Microscope (TEM)

Similiar to SEM a TEM forms an image of a sample by electron interaction, but as the name suggest the electrons are transmitted through the sample, greatly expanding the characterization possibilities. The needed electron transparency of the sample gives some restrictions, it has to be ultrathin in the range of 100 nm. To create ultrathin slices of the inserts in this thesis, focused ion beam (*FIB*) technique is used.

TEM is operated in two modes. In the conventional TEM mode a larger area of the sample is illuminated by the electron beam and by lenses pictured on a screen either producing an image or a diffraction pattern. In scanning TEM (STEM) mode the electron beam is focused on a specific point on the surface and will sequentially map the surface in a raster pattern forming an image by plotting the intensity as a function of beam location.

TEM and STEM makes it possible to study different areas of the slice as grain and crystal structure from contrast. In this thesis the following techniques has been used;
Calculation of lattice parameters by TEM from diffraction patterns by selected area electron diffraction (*SAED*). In the STEM mode maps of elements been created by X-ray energy-dispersive spectrum (*XEDS* or *EDX*), by the same mechanism as in *EDX* for SEM. [13]

4.4 Focused Ion Beam (FIB)

Focused Ion Beam for TEM preparation is very useful and makes it possible to study a cross section of the inserts in detail. The FIB setup at Lund NanoLab consists of a vacuum chamber with an ion beam gun accompanied by a SEM for visual aid during operation, a rod for mechanically moving objects and a gas source for deposition.
A beam of Ga^+ ions are accelerated hitting the sample surface sputtering a small amount of material, carving out the desired lamella. By releasing a gas containing platinum, the ion beam will work as a catalyst for depositing the platinum metal at the beam impact

position used for protection or glue. In the instrument there is a rod for moving the sample to the TEM holder.

In Figure 14 the sequential approach for preparing a sample and attaching it to the TEM holder is shown.

a) Location of the lamella is chosen, and protected with a string of platina.

b) To get the sample out, rectangular areas are sputtered.

c) This is performed in a step way fashion creating a slope.

d) Same thing is done on the other side.

e) The slope is needed for cutting the lamella off.

f) The rod is attached to the lamella and glued on with platina and the last side is cut off.

g) The lamella is mechanically moved from the sample to the TEM holder also located in the vacuum chamber.

h) The TEM holder is about $50\mu m$ wide.

i) The lamella is glued onto the holder and cut off from the rod.

j) The lamella is too thick and needs to be polished.

k) FIB is used to polish both of the sides.

l) This is repeated a number of times to reach a thickness about 100 nm. The platina is a good protection during polishing.

m) The thickness has to be repeatedly checked "from above".

n) The lamella is $16\mu m$ long, with a $12\mu m$ of coating.

o) $11\mu m$ wide.

p) In this case the lamella is about $185nm$ to $553nm$ in thickness.

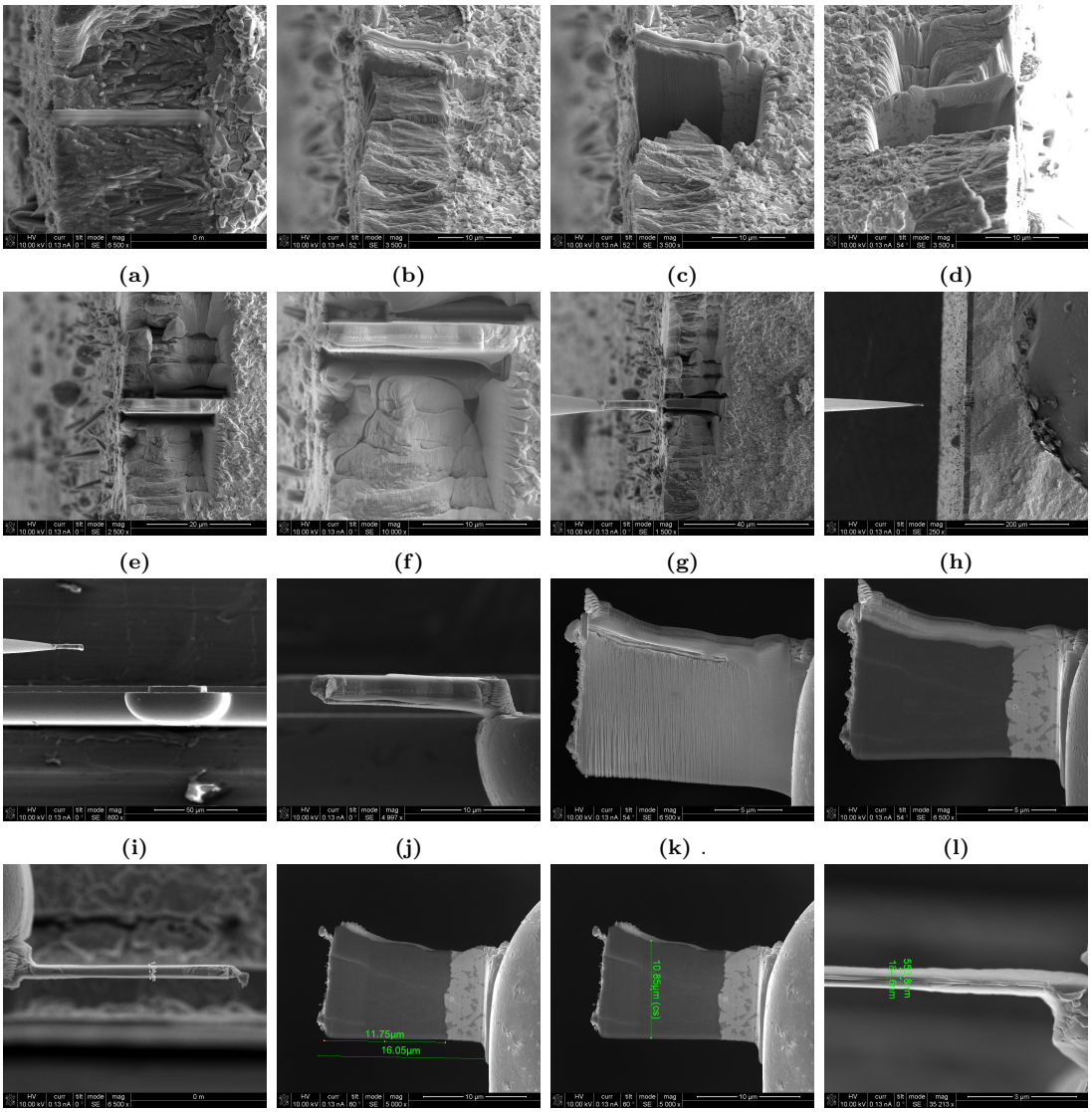

(a) **(b)** **(c)** **(d)**

(e) **(f)** **(g)** **(h)**

(i) **(j)** **(k)** . **(l)**

(m) **(n)** **(o)** **(p)**

Figure 14 FIB sequential steps.

5 Design of Experiment (DoE)

The goal of this thesis is to create a general knowledge basis of the growth parameters of Ti(C,O) on different substrates with the optimization for a favorable bonding layer in mind. The parameter space of the experiments are limited by the present CVD system at Seco Tools.

5.1 Substrates

Six substrates has been coated; *Cemented carbide* (WC/Co), used as the body for all the inserts, three of these were placed radially (inner, middle, outer) to create a thickness profile. *Cubic Boron Nitride* (c-BN) from Amborite, close to diamond in hardness with a similar crystal structure. *Titanium Nitrade* (TiN), fine-grained and coarse-grained *Titanium Carbonitride* Ti(C,N), (8 micron layer on a WC/Co body). And a *chromium* layer on WC/Co body.

5.2 MODDE

MODDE (**MOD**eling and **DE**sign) is a software by Umetrics.

The conventional approach for setting up experiments is the step method, optimizing one factor at the time. With this method it is easy to follow every step along the way and couple every response to a factor. The big downside is not only that it is inefficient and interesting spots in the design space may be missed. Letting an algorithm choose your experiments will also exclude any prejudices that may hinder the big discoveries. Instead the software MODDE will suggest that the experiments are chosen in such a way that the space spanned of the factors, is optimized for the best coverage given the number of experiments. By quantifying experiment responses in MODDE they are mapped onto this space by polynomials with a certain precision. If a combination of optimum responses are sought for MODDE will calculate the sweet spots.

5.2.1 Factors

For a easy comparison of the samples the time in the furnace have been set to 6 hours. This way all samples will have time to develop their growth. As earlier described the variable parameters are:

Ratio

The mass flow gauges have a range of 0.5 to 9.6 ml liquid/min for $TiCl_4$ and 0.25 to 5 liter gas/min for CO. The stoichiometric relation for $TiCl_4/CO$ is 5/1 liters gas. Three ratios where chosen:

Supersaturation of CO;
$5[l/min]$ of CO and $5[ml/min]$ of $TiCl_4$ giving a molar relation of 0.2.
Stochiometric relation;
$1.5[l/min]$ of CO and $7.5[ml/min]$ of $TiCl_4$ giving a molar relation of 1.
Supersaturation of $TiCl_4$;
$0.38[l/min]$ of CO and $9.6[ml/min]$ of $TiCl_4$ giving a molar relation of 5.

Temperature

The tempearture range of the CVD system is 860°C to 1000°C. A lower temperature is preferential to not risk interdiffusion, which can be a problem if Ti(C,O) is deposited on

the cemented carbide at 1000°.

Pressure
The range of pressure is 50 mbar to 500 mbar.

Hydrogen gas
The range of hydrogen gas is 6 to 120 $[l/min]$ and thus will always be in excess.

5.2.2 Responses

To quantify responses for MODDE is not straightforward and many important morphological responses are subjective. An advanced image analysis algorithm or an artificial intelligence looking for patterns in the SEM pictures would be of a good use.
The *Deposition rate* is easily quantified, the average thickness of the innermost, middle and outer cemented carbide sample was divided by time in the furnace ($[\mu m/h]$). A factor that needs to be considered during industrial production of inserts is an even growth of the inserts at all positions on the crucible, therefore the *variance coefficient* (defined as the deviation from the mean squared in percent) is set as an response.
Another easily quantified data point is the *lattice parameter*, calculated from the XRD measurements. The measurements yields a precision of about 3 decimals. The lattice parameter is an important indication of carbon and oxygen composition.
The *Texture Coefficients* calculated from the relative presence of the first 8 orientations measured by XRD.
For a way to quantify the morphology the response "flake length" was invented by measuring the length of flakes using the software ImageJ. ImageJ has a script for automatically measuring the size of objects by changing the contrast. This was unfortunately hard to do because the flakes touch each other too much and it ended up being faster measuring them by hand using ImageJ's measurement tools, see Figure 15.

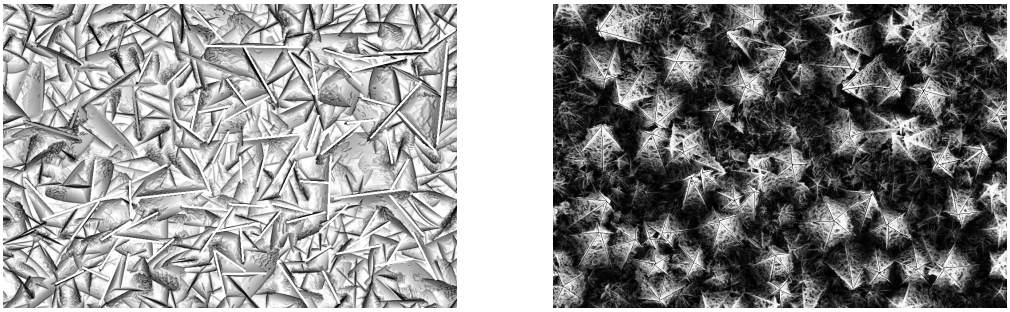

(a) Example of surface with flakes, colors inverted. In ImageJ.

(b) Example of surface with stars. In ImageJ.

Figure 15 Measuring of "flake length".

In Figure 15 the flakes are covered with a gray or white line to keep track of counted flake or not. Then the average length and variance is calculated.

5.3 Experiments

5.3.1 Screening test

With above mentioned factors, MODDE calculated a number of experiments. *Ratio* was chosen to be a "multilevel quantity". MODDE have different design options but due to the discrete aspect of the *ratio*, a "reduced combinatorial design" was chosen. A screening

test is supposed to limit the number of factors for future tests, but because all results are interesting and rather time consuming, the screening tests are the main tests.

Table 1 Screening test. D is repeated for measurement of precision.

Exp. name	Ratio	Temperature [$°C$]	Pressure [mbar]	H_2 [ml]
A	0.2	860	50	120
B	0.2	1000	500	6
C	0.2	1000	50	6
D	1	1000	50	120
E	5	1000	500	120
F	1	860	500	120
G	5	860	500	6
H	1	860	500	6

5.3.2 Focusing tests

An evaluation of the screening test, gave insights to the importance of factors. By choosing a couple of experiments in an interesting area, the algorithm will calculate better model terms and give a better prediction.

Table 2 Focusing test.

Exp. name	Ratio	Temperature [$°C$]	Pressure [mbar]	H_2 [ml]
I	0.5	1000	50	32
J	0.2	1000	500	120
K	1	1000	500	63
L	2	1000	500	96
M	3	1000	500	6
N	1	1000	500	120
O	1	1000	50	63
P	1	930	500	120

5.3.3 Fitting of model

MODDE suggests number of model terms depending on number of experiments in the screening test. Using linear regression analysis a polynomial is fitted to the data points. As experiments are carried out the precision of the model is increased and more terms can be added while reviewing the fit.

Starting with linear and quadratic terms for all factors. The focusing test expanded the information of the ratio and hydrogen relation, and a interaction term between these two could be included.

Not all responses have a good fit and some has to be disregarded. Reasons are low precision in the measurements, complex parameter relations and stochastic nature of the responses.

6 Result

All analysis are performed on the WC/Co substrate if nothing else is indicated. In Table 4 in Appendix μ a summary of all samples can be found. All texture coefficients are found in Figure 37 Appendix μ. Process parameters and their relation to texture formation is highlighted in the result and discussed in "9. Discussion and Conclusion".

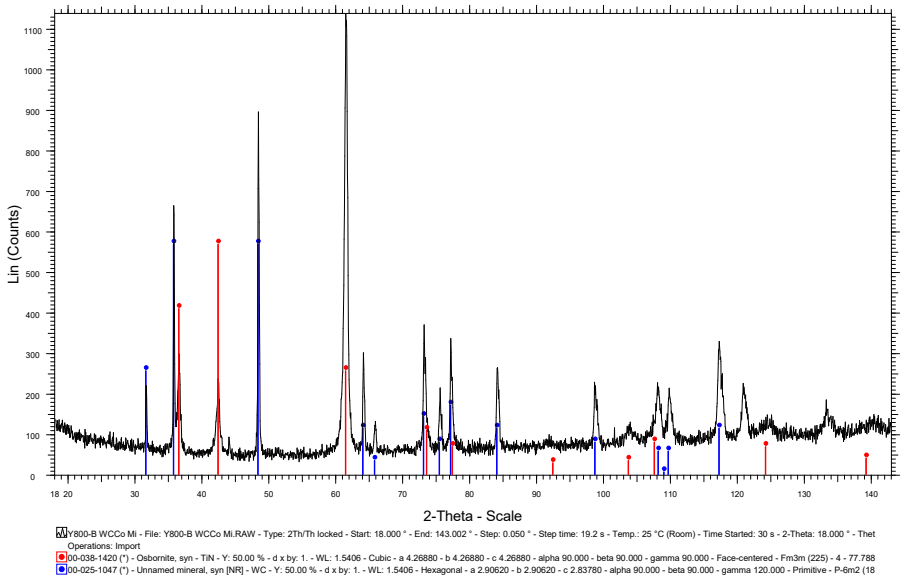

Figure 16 XRD diffractogram of sample B. Blue lines indicate WC/Co and red lines Ti(C,N) orientations. A large peak for the {220} orientation can be seen for 2θ=61.4°. See Appendix μ Figure 37 for texture coefficient.

6.1 Crystal orientations

The texture coefficient show no signs of one specific orientation growth for any sample, see Appendix μ, Figure 37. MODDE is indicating a bad measure of prediction. It is demonstrated by a large probability for a non significant model for the orientations and the repetition of D show a low reproducibility (Appendix μ see Figure 37). In Figure 17 SEM images of sample B are displayed. The surface in 17(d) visualize a characteristic feature of Ti(C,O), small solid crystal flakes with lack of order and parallelity.

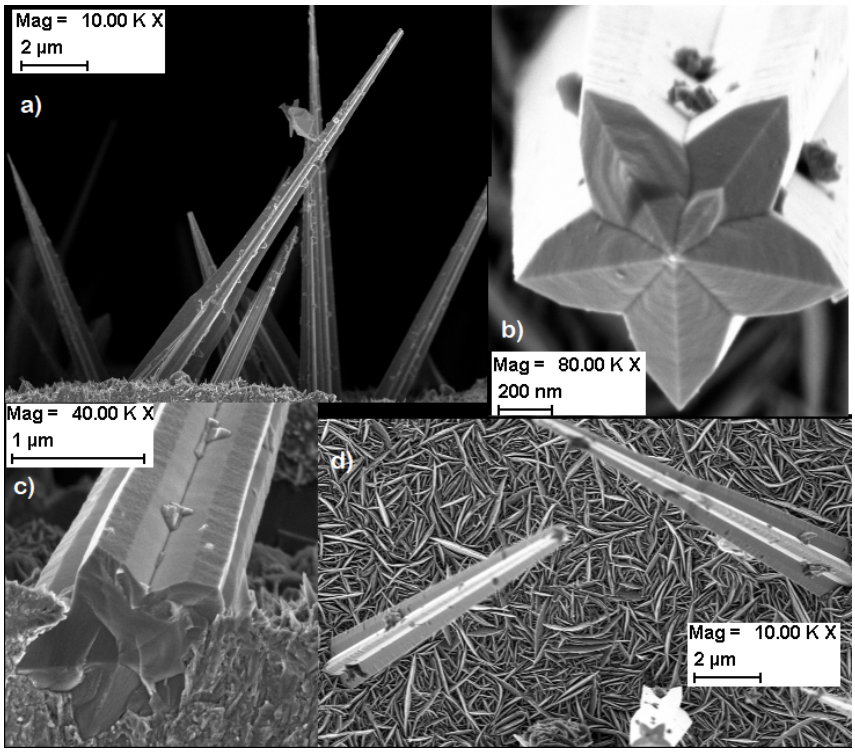

Figure 17 B, Five-ling twinned crystals or *stars*.

6.1.1 Five-ling multiple twinned crystals or Stars

In sample B (Figure 17) same stars obtained in TiN by Cheng et al. [16] and Ti(C,N) by Sun et al. [17] are observed, suggesting same growth mechanisms.

The stars nucleates without any indication deep in the growth stage (Figure 17(c)) and can be as tall as 10 μm (Figure 17(a)). They possess almost a vertical growth and do not seem to get sharper without kinks (Figure 17(a)). Cheng report the stars to grow in the [220]-direction which is confirmed the by XRD made on B, see Figure 16. The {220} orientation is thus an indication of five-ling twinned crystals or decahedrons.

In Figure 16 both the {111} (2θ=36.4°) and {200} (2θ=42.3°) orientations are very small, even more obvious for the texture coefficent, see Figure 37 in Appendix μ. {111} is the vertical twin boundary, and would not show up in XRD. {200} is a potential candidate for a side surface orientation of the flakes or an indication of this surface being non-favorable. In Ti(C,N) the {200} is the side surface orientation of the 211 grain, see Figure 3. These two orientations are more or less non-existent for all samples, see Appendix μ, Figure 37. Sample B is the only one with obtuse SAG angles like Figure 17, other samples exhibiting fivefold multiple twinned crystals structures are of the type in Figure 19b or in Figure 23.

6.1.2 The {220} orientation

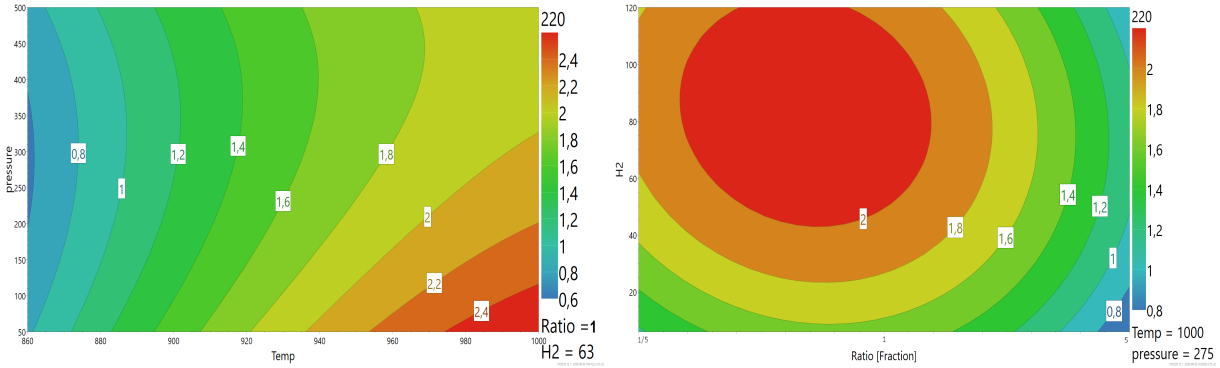

(a) The {220} response as a function of temperature (x-axis) and pressure (y-axis). Ratio=1, H_2=63 l/min.

(b) The {220} response as a function of hydrogen (y-axis) and ratio(x-axis). Temperature=1000°, pressure=500mbar.

Figure 18 The texture coefficient of {220} response, barely acceptable model fit and estimate of future prediction. Result should be taken as tendencies. {220} is the horizontal plane of stars.

In Figure 18 the TC coefficient of {220} orientation is plotted as a function of temperature and pressure in 18a, and ratio of $TiCl_4$/CO and H_2 in 18b. Note that all responses that are equal to 1 (blue color in Figure 18) indicates a random distribution of orientations and a higher number indicates a larger presence of the orientation. These responses roughly maps to the presence of "pine trees" (Figure 19b). See Figure 22 for surface texture mapped to the deposition rate, N K and L are all exhibiting pine trees.

Figure 18a demonstrates temperature as a precursor for decahedral nuclei. In the same figure pressure is indicated as having a small inverse relation to the {220} planes, this relation is within the error bars and the {220} orientation is still preferable at high temperature and pressure (TC≈2). Stars and pine trees only occur at high pressures, this indicates that the decahedral nuclei are present at the lower pressure but the high pressure is necessary for the "arms" of the decahedral nuclei to spur into growth. Hydrogen is strongly correlated to the number of stars in Figure 18b. The result indicate that the number of stars and their nuclei are coupled to hydrogen while size is coupled to pressure.

6.1.3 Pine trees

Cheng et al [16] found that a higher temperature and decreased partial pressure of $TiCl_4$ incline stars to be more pentagonal, i.e. the angle at the SAG boundary (Figure 9) are more obtuse. For Ti(C,O) the largest and most pentagonal stars occur at supersaturation of CO (less $TiCl_4$), high temperature and low H_2 flow, see Figure 19a, confirming the result of Cheng.

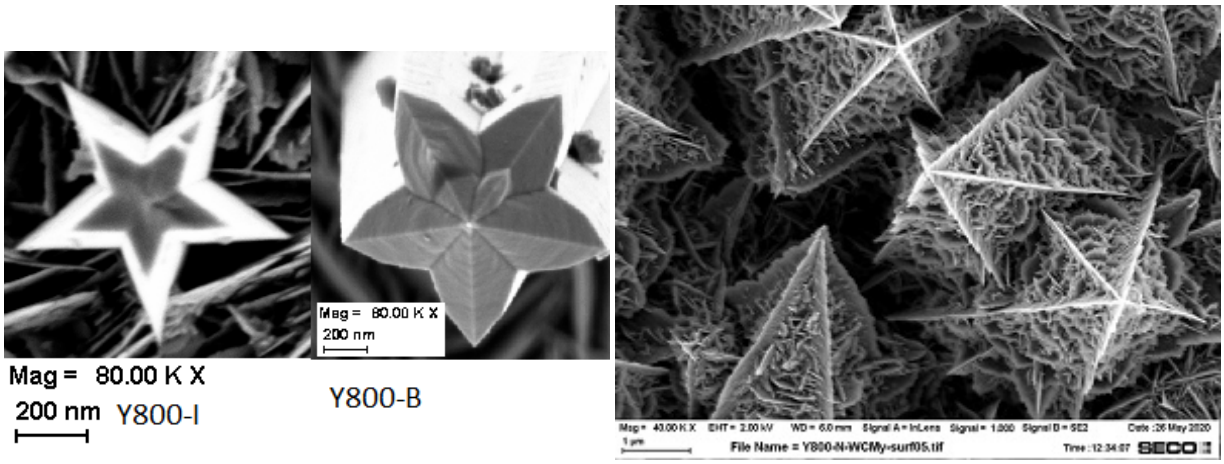

(a) (b)

Figure 19 Different kinds of star formation. Pressure = 500 mbar, Temperature = 1000°.

Sample B, Figure 19a, exhibiting large and sparse stars was generated in an environment of low hydrogen and a saturation of CO. When increasing hydrogen and $TiCl_4$ as sample I (the star to the left in 19a), the stars are small, sparse and have a sharper angle at the SAG boundary. At stoichiometry and more hydrogen like the samples K, L and N large "pine trees" are generated (see Figure 19b). These have very thin arms, with small protrusions and covers the all of the surface.

6.2 Temperature

From Arrhenius plot (21b) and of the discrete change in morphological structure between Figure 21c and 21e, it can be concluded that there are at least two growth mechanisms present. Thus a change in activation energy at a temperature between 930°C and 1000°C.

6.2.1 Low temperature samples

None of the samples at 860°C (A, F, G and H, see Table 4), exhibited any larger crystals; they are fine grained and uniform, see Figure 20a and 20b. The deposition rate has a negligible dependency on pressure, a moderate on ratio of $TiCl_4$/CO and depends mainly on hydrogen and temperature, see Figure 20c.

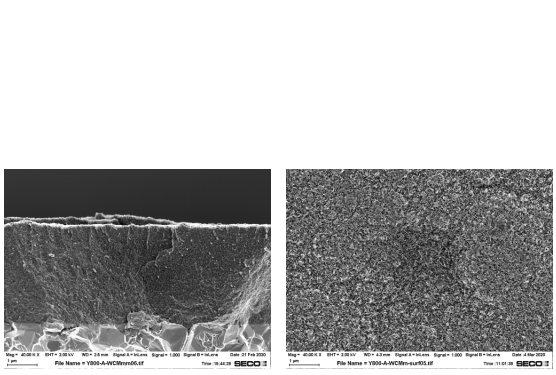

(a) Sample "A" fine grained cross section. **(b)** Sample "A" feather-like surface.

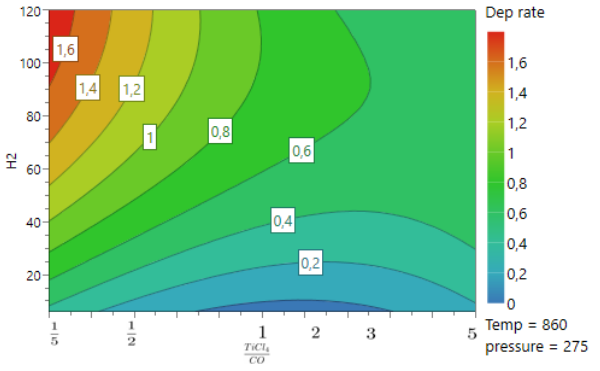

(c) Map of deposition rate. Temperature = 860°C, Pressure = 275 mbar.

Figure 20 Small grain, feather-like structure. Typical for all samples at 860°C.

The grain size of low temperature samples are small (Figure 20), the activation energy for growth of any larger crystal structures are not large enough and the XRD tells of no

favorable orientation, see Figure 37 Appendix μ. From the cross section in 20a it can be concluded that only the nucleation stage is prevalent. The crystals are ultra thin and about 75 nm in length.

6.2.2 Growth rate

F, P and N (see Table 4) are chosen for calculation of Arrhenius equation (1), possessing same process parameters except temperature. P had a deposition time of 1 hour, the homogeneity of structure of the cross section might be retained during a 6 hour deposition time but it is hard to know without letting it grow. It can be seen F (Figure 21c) is different from N (Figure 21e) which indicates a different growth mechanism.

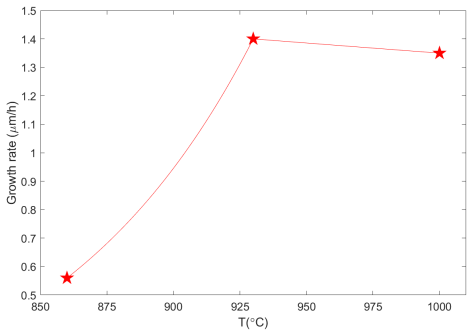

(a) Growth rate as a function of temperature.

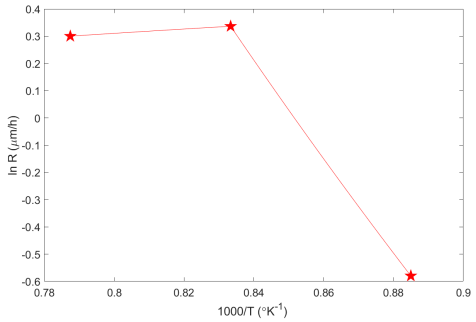

(b) Arrhenius plot

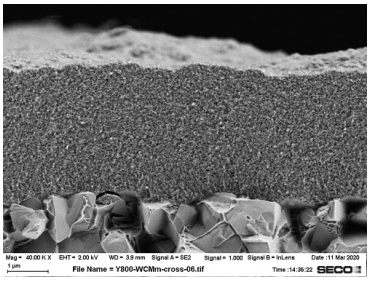

(c) Cross section of F, T=860°. Thickness = 3.4μm, deposition time 6 hours.

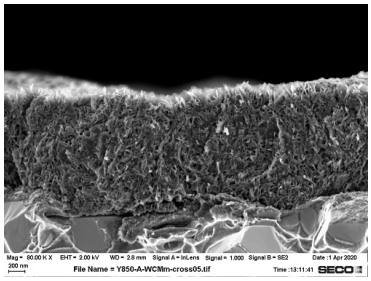

(d) Cross section of P, T=930°. Thickness = 1.4μm, deposition time 1 hour.

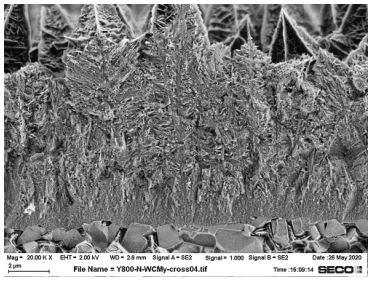

(e) Cross section of N, Thickness = 8.1μm, deposition time 6 hours. T=1000°

Figure 21 The lines between the data point (pentagrams) are fitted with an exponential curve. Stoichiometric relation between $TiCl_4$ and CO, Pressure = 500 mbar, 120 l/min hydrogen.

There are too few data points to get a reliable activation energy. Figure 21b displays a negative activation energy, N has a smaller growth rate than P. If this is due to the deposition time or different growth rates are hard to know. Orientation-wise a transition from a relatively equal distribution to more of {220} can be observed, see Figure 18a.

6.2.3 High temperature samples

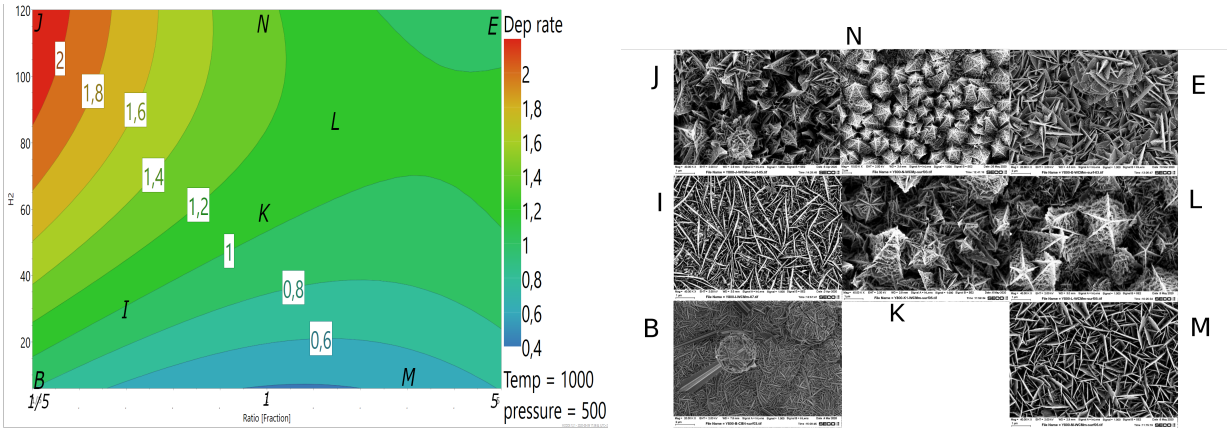

(a) Deposition rate. Ratio on the x-axis and hydrogen on the y-axis ranging from 6 to 120 l/min.

(b) Surfaces images of the high temperature samples their letter is mapped onto the deposition rate map.

Figure 22 Map of deposition rate with corresponding surfaces. T=1000°, P=500mbar.

Compared to the low temperature samples the high temperature samples show a larger variety of morphology (Figure 22b). Surface morphology are mapped onto the map of deposition rate. By comparing B (Figure 17a) to J (Figure 23) it can be seen that an increase in nucleation sites due to increased partial pressure of hydrogen. The deposition rate for J is more than three times the one of B, see Table 4 in Appendix μ.

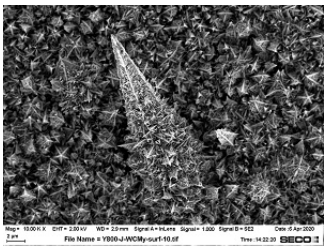

Figure 23 J "star with nucleation sites."

In the lower left corner of 22a (sample B and I) the flakes are long and curved. N, L and K all look similar, exhibiting pine trees 19b. E has a moderate deposition rate, flakes with side protrusions and have much in common with the lower pressure samples, see Section 6.2.4. M has a low deposition rate with fine flakes. All samples show varying levels of the fine grained nucleation stage and larger grained growth stage. The N, K, L samples on the Ti(C,N) substrates did not exhibit any pine trees see Figure 31a and 31c and section 7.1.

6.2.4 Low pressure samples

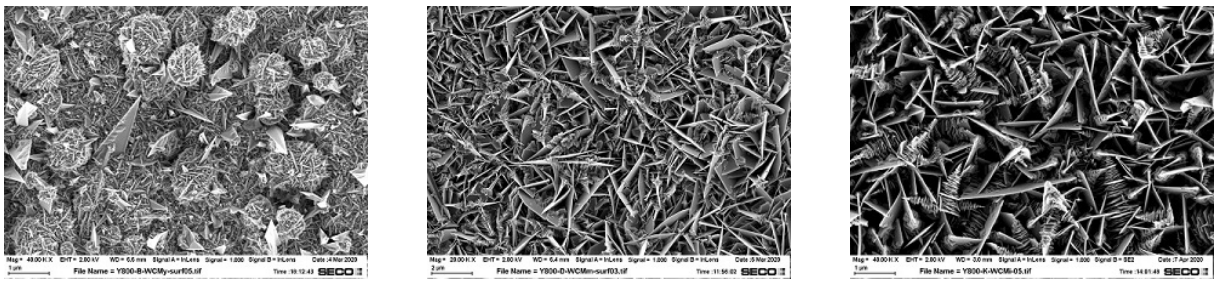

(a) C **(b)** D **(c)** O

Figure 24 Low pressure samples, P=50mbar.

The low pressure samples in Figure 24, exhibit a different type of surface than their corresponding high pressure samples. Apart from the pressure, sample C have the same process parameters as B, D as N and O as K (See Appendix μ, Table 4). Pressure effecting the boundary thickness have thus a large effect on morphology as foreseen by Equation 2.

No long structures as stars or pine trees exists. C is rather disordered with "balls" and "spikes". D and O have flakes with lots of side protrusions and the surface morphology is the same independent of substrate, see the Ti(C,N) substrate Figure 32.

6.3 TEM Analysis

TEM was performed on sample B with fine grained Ti(C,N) as intermediate layer. This sample was chosen because its interesting star formation (Figure 17) and a Ti(C,N) layer for reference. Compared to XRD the TEM measurements are from a 90° angle cross-section of the insert, see the lamella in the Section 4.4. This made it possible to study different sections in the growth of Ti(C,O).

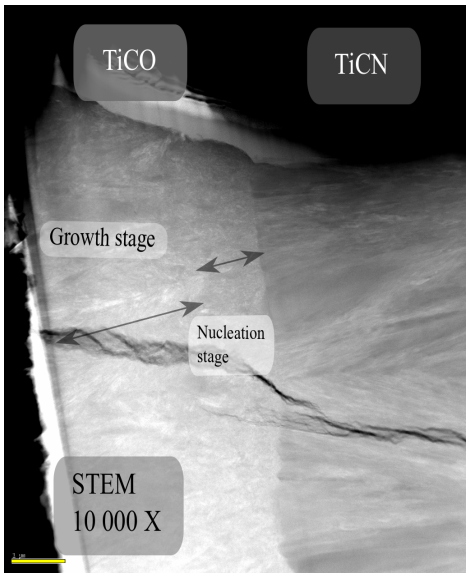

(a) STEM, nucleation and growth stage visualized.

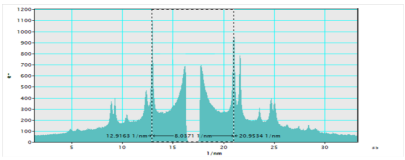

(b) Contrast profile from the diffractogram beneath, measurements of circle-diameters in table 3.

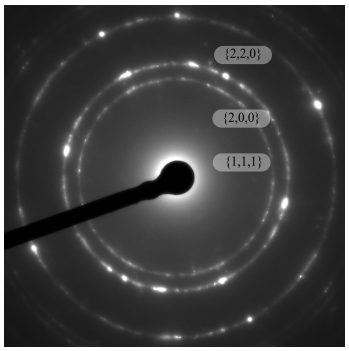

(c) SAED pattern.

Figure 25 STEM and TEM pictures

The sharp rings in 25c indicates a relatively homogeneous composition of the coating. In Figure 25b the radius of the rings (reciprocal nanometers) has been measured and collected in Table 3. This yields the lattice spacing $d_{h,k,l}$ and the unit cell parameter a can be calculated according:

$$d_{h,k,l} = \frac{a}{h^2 + k^2 + l^2} \tag{10}$$

Table 3 Data collected from figure 25b.

Circle diameter [1/nm]	Orientation	$h^2 + k^2 + l^2$	**a** [Å]
8.05929	{1,1,1}	$\sqrt{3}$	4.302
9.2767	{2,0,0}	2	4.312
13.0979	{2,2,0}	$\sqrt{8}$	4.319
15.4032	{3,1,1}	$\sqrt{11}$	4.306
16.1059	{2,2,2}	$\sqrt{12}$	4.302
18.6876	{4,0,0}	4	4.281
20.0231	{3,3,1}	$\sqrt{19}$	4.302
20.7561	{4,2,0}	$\sqrt{20}$	4.309
22.6982	{4,2,2}	$\sqrt{24}$	4.317
24.2457	{5,1,1}	$\sqrt{27}$	4.286

Mean lattice parameter is 4.304 Å, from Table 3. Platinum was used as reference material and unit cell calculations showed a precision within 1%. The standard deviation is relatively large in Table 3. XRD have a better precision and will be used for analysis.

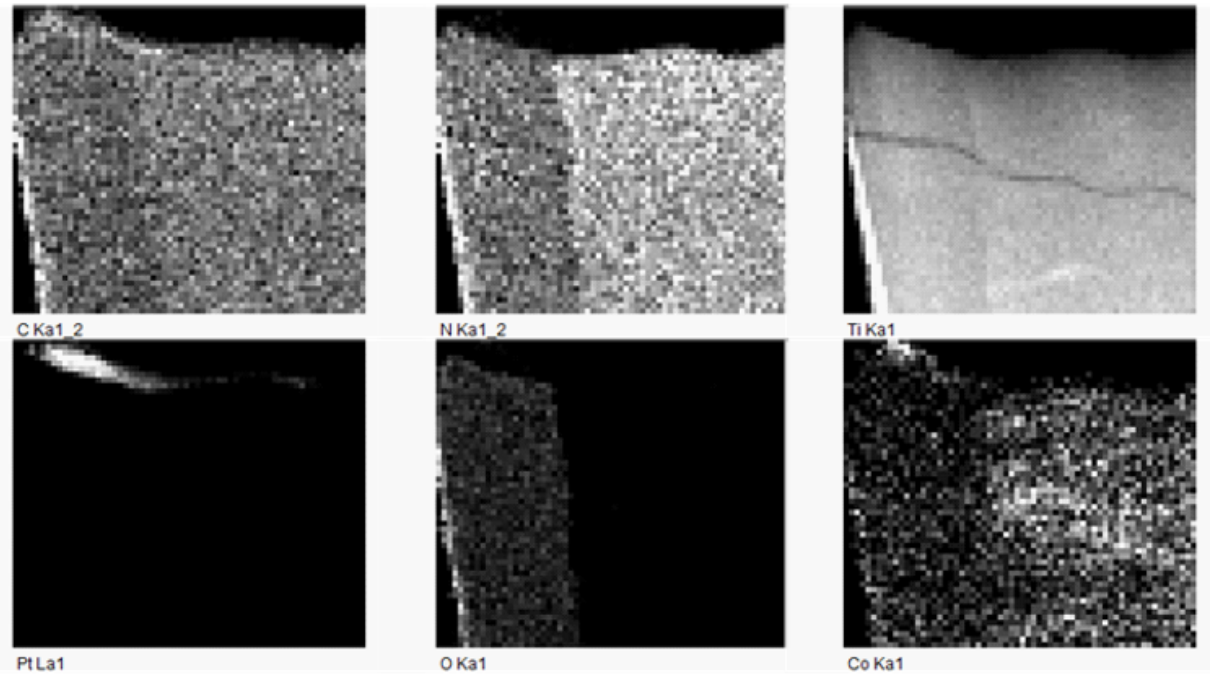

Figure 26 EDS by STEM (same window as figure 25a, Ti(C,O) to the left, Ti(C,N) to the right). Every picture marked by searched for element and X-ray wavelength (Cu Kα1 and Cu Kα2).

The result from EDS in Figure 26 show the relative presence of carbon, nitrogen, titanium, platinum, oxygen and cobalt. Heavier elements have a tendency to be overestimated while light elements like carbon, nitrogen and oxygen are underestimated. Also, energy overlap increases the problem of quantifying light elements. It can be concluded: relatively less carbon and titanium in Ti(C,O) compared to Ti(C,N); more oxygen in Ti(C,O) than nitrogen in Ti(C,N). No oxygen in Ti(C,N) and probably no nitrogen in Ti(C,O). A "plume" of cobalt can be seen in Ti(C,N) which does not continue into Ti(C,O), unclear if made before or after annealing during deposition of Ti(C,O).

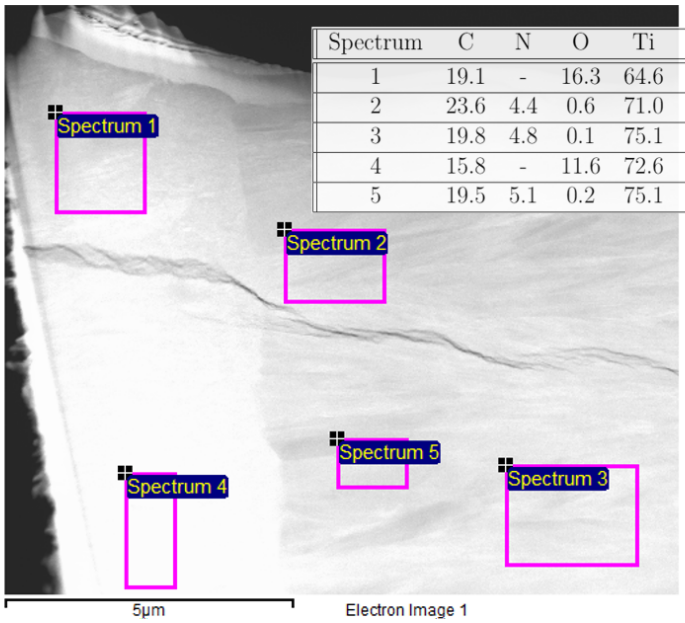

Spectrum	C	N	O	Ti	Co
1	19.1	-	16.3	64.6	-
2	23.6	4.4	0.6	71.0	0.3
3	19.8	4.8	0.1	75.1	0.2
4	15.8	-	11.6	72.6	-
5	19.5	5.1	0.2	75.1	0.1

Figure 27 EDS performed on 5 areas, result in atomic percent in table, "-" not measured for. (Same window as figure 25a, Ti(C,O) to the left, Ti(C,N) to the right).

In figure 27 the mean composition for Ti(C,O): 18%C 14%O and 69% Ti → $\underline{\text{Ti}(\text{C}_{0.55},\text{O}_{0.45})_{0.46}}$. Ti(C,N): 21% C, 5% N, 0.3% O, 74% Ti and 0.2% Co→ $\underline{\text{Ti}(\text{C}_{0.8},\text{N}_{0.2})_{0.35}}$.

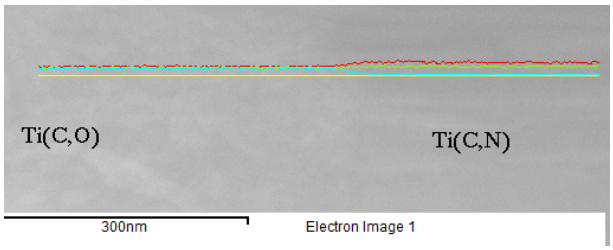

(a) EDS linescan from Ti(C,O) to Ti(C,N) different colors are different elements see 28b.

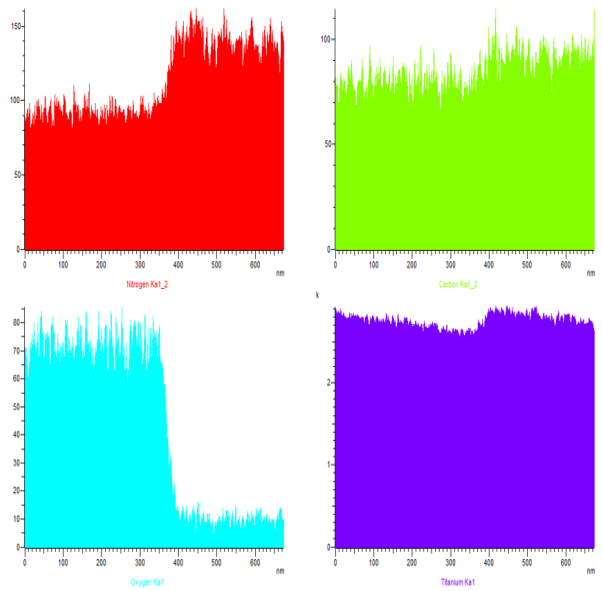

(b) Nitrogen in red, carbon in green, oxygen light blue and titanium in purple. Notice the different y-axis (intensity). x-axis in nm.

Figure 28 Line scanning (EDS)

In Figure 28a and 28b, the boundary between Ti(C,O) and Ti(C,N) is studied. As

described earlier there is an overlap between nitrogen and oxygen and they have probably not diffused passed the border. This study also shows a small but significant reduction in carbon in Ti(C,O). It looks like titanium have a linear increase as you move towards the surface. Less titanium in Ti(C,O) than in Ti(C,N).

6.3.1 Comment on the TEM Result

As seen in Figure 27 there is a large variation of composition. The composition in Ti(C,N) is known and could be used as a reference. von Fieandt [5] reports a composition of $Ti(C_{0.6},N_{0.4})_{0.8}$, and it can be concluded heavier elements are overestimated. This can be due to a bad calibration of the TEM or a nonuniform thickness of the lamella. C, N and O have close X-ray peaks in EDS and it is known to hold a low precision for light elements. In this case X-ray photoelectron spectroscopy (XPS) would be more precise.

However, the results suggests a larger presence of oxygen in Ti(C,O) compared to nitrogen in Ti(C,N). A result supported by Ruppi et al [8] suggesting oxygen surpass nitrogen in atomic percent as carbon monoxide is increasingly added.

6.4 Smoothness

The model for the variance coefficient of radial thickness demonstrates barely a significant model. "Smoothness" is inherently a stochastic variable and relays on three non precision measurements of the thickness of the inserts radially placed by hand. The coefficients of the terms indicates temperature to be nonsignificant.

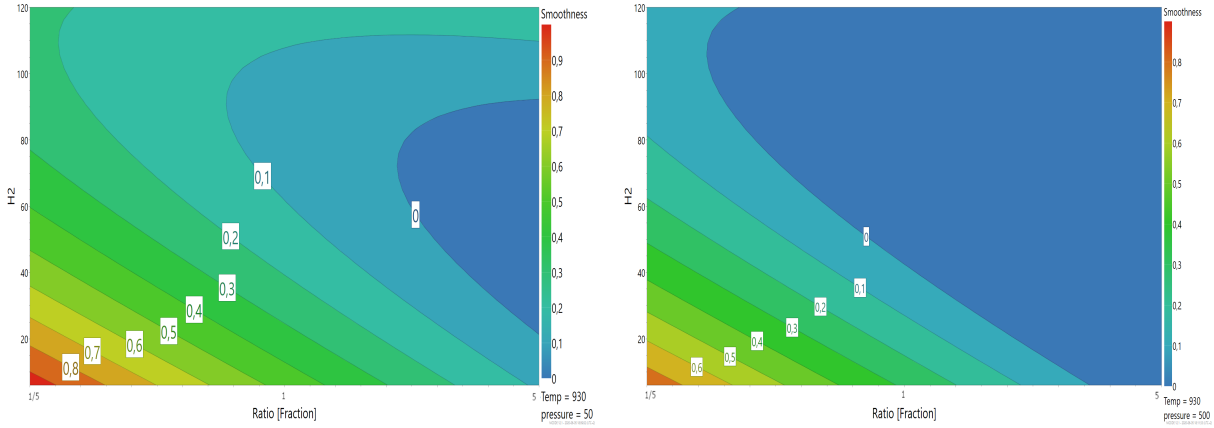

(a) Variance coefficient. y-axis hydrogen, x-axis ratio. T=930°C, P=50mbar.

(b) Variance coefficient. y-axis hydrogen, x-axis ratio. T=930°C, P=500mbar.

Figure 29 "Smoothness", variance coefficient of the radial thickness.

In Figure 29, blue indicates "smoothness=0", the three radial samples exhibit equal thickness. It can be concluded more $TiCl_4$ in combination with a moderate flow of H_2 results in a smooth surface. Comparison of them indicates higher pressure will result in a smoother surface. These results could possible be made general for all coatings in the CVD system at Seco Tools, especially with more data and be a guideline in creating a small variance of thickness.

6.5 Unit cell

The model for the unit cell displays a relatively significant model and a range of 4.27 to 4.29 Å, see Figure 30. See every unit cell parameter for in Appendix μ in Table 4. The lattice parameter is an indication of the composition, see Equation 5.

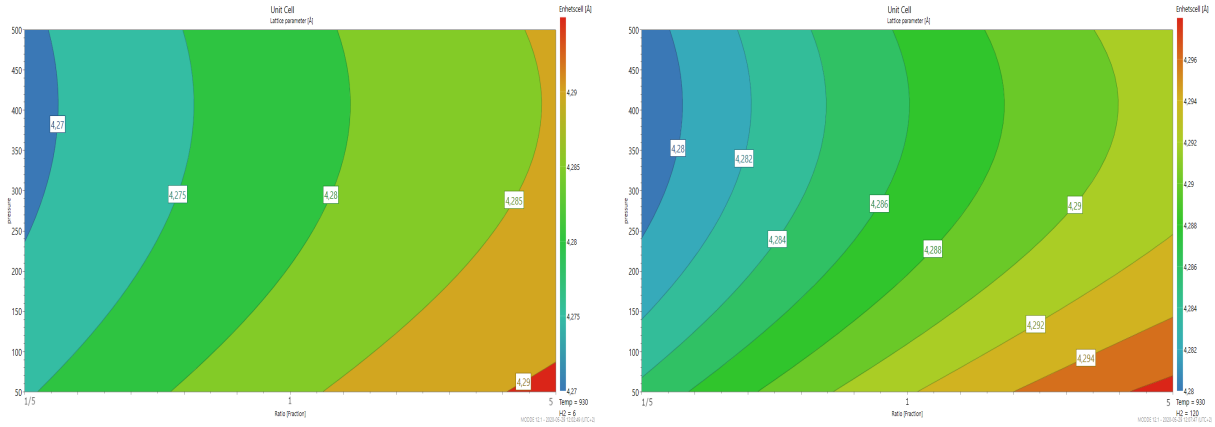

(a) Lattice parameter, pressure on y-axis, ratio on x-axis. T=930°C, H_2=6 l/min.

(b) Lattice parameter, pressure on y-axis, ratio on x-axis. T=930°C, H_2=120 l/min.

Figure 30 Lattice parameter **a** [Å].

Temperature have a minor relevance for the lattice parameter see Figure 30. The most significant factor is the ratio of $TiCl_4$/CO. Higher pressure will result in a smaller unit cell. For the hydrogen dependency, compare Figure 30a (6 l/min hydrogen) and Figure 30b (120 l/min hydrogen). The increase of hydrogen will shift the Ti(C,O) unit cell with about 0.01 Å.

7 Substrates

Generally there is not a large substrate dependence. The biggest dependence of the morphology can be observed on the Ti(C,N) substrates. This is clear on sample N, K and L on the fine and coarse Ti(C,N) substrates (see Table 4 in Appendix μ). On c-BN and TiN a higher presence of stars can be observed, these substrates have in common to containing part of either TiN, TiC or Ti(C,N). Some of the observed change of surface structure morphology could possibly be attributed to the substrate surface topology.

7.1 Ti(C,N)

Sample N, K, L, E, D and O (see Table 4) all exhibit epitaxial growth on the Ti(C,N) substrates. They have in common a temperature at 1000°C, ratio of $TiCl_4/CO \geq 1$ and a hydrogen flow of 63 l/min or more. The pine trees on N, K and L are absent on the Ti(C,N) substrate samples and are instead exhibiting flakes as in Figure 31. In these samples the thickness of the coating also stand out. L demonstrate an approximately 25% thinner coating than the coating on hard metal, this is probably not due to a lower growth rate but a more dense coating. The other samples exhibit similar surface morphology independent of substrate, see Figure 32.

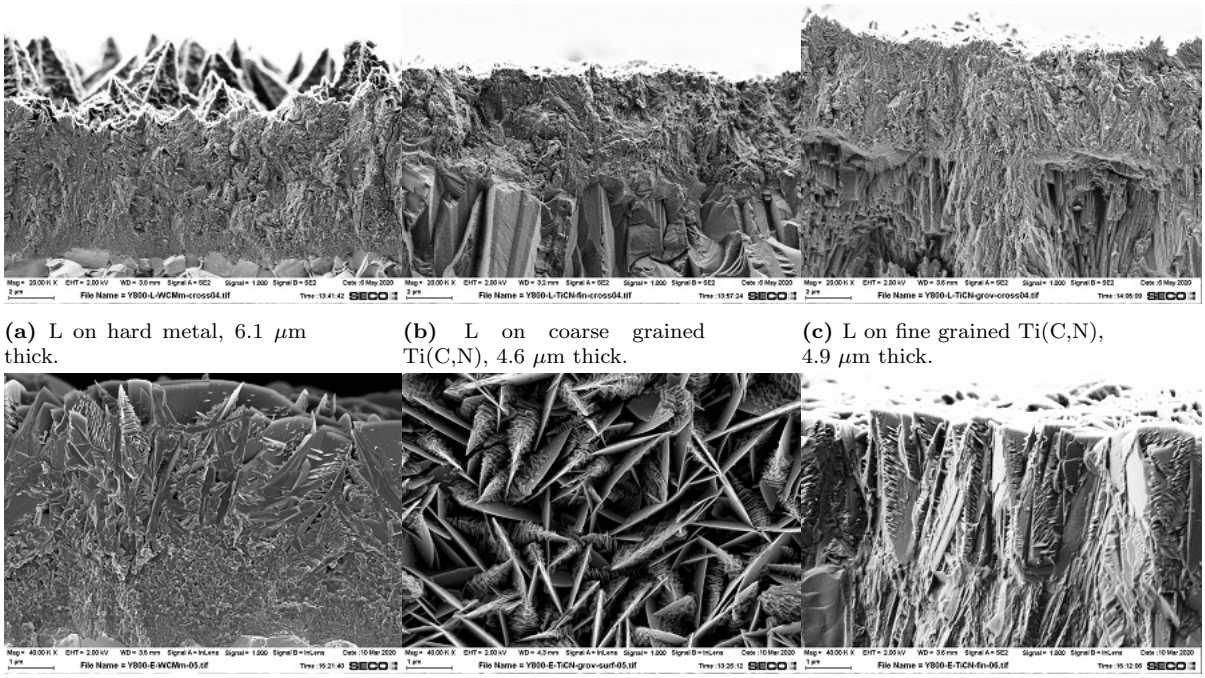

(a) L on hard metal, 6.1 μm thick.

(b) L on coarse grained Ti(C,N), 4.6 μm thick.

(c) L on fine grained Ti(C,N), 4.9 μm thick.

(d) E on hard metal, 5.5 μm thick.

(e) E on coarse grained Ti(C,N), 3.5 μm thick.

(f) E on fine grained Ti(C,N), 6.7 μm thick.

Figure 31 Sample L and E, different morphology and thickness on Ti(C,N).

Sample E on fine grained Ti(C,N) coating is 25% thicker while E on coarse grained Ti(C,N) is 35% thinner than the respective coating on WC/Co (see Figure 31), probably due to the lower deposition rate on all E samples (see Appendix μ 4), the crystal morphology will have a bigger impact on the thickness.

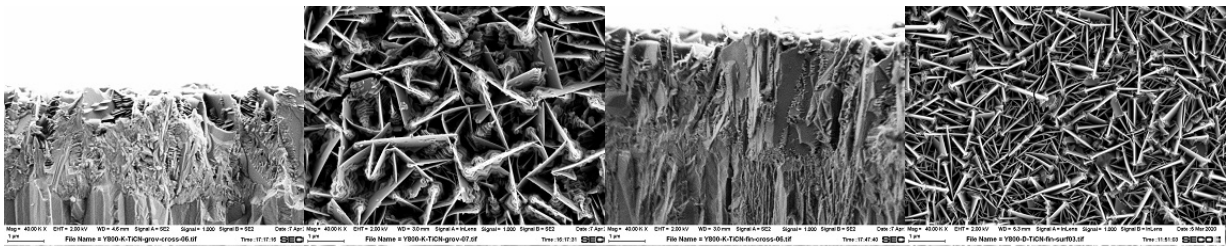

(a) O, coarse grain Ti(C,N), 2.5 μm thick.

(b) O, coarse grained Ti(C,N),

(c) O, fine grain Ti(C,N), 3.4 μm thick.

(d) Surface of D fine grain Ti(C,N).

Figure 32 O and D. Characteristic morphology of fine and coarse grained Ti(C,N) on D, O and E.

7.2 Chromium

There is no clear coupling to process parameters for interdiffusion of chromium. Chromium pores are present in the fine grained morphology, F and G but not in A. P has the largest pores of chromium. At O, (see 33c, in red circles) pores are visible but not at other high temperature samples. See Figure 33.

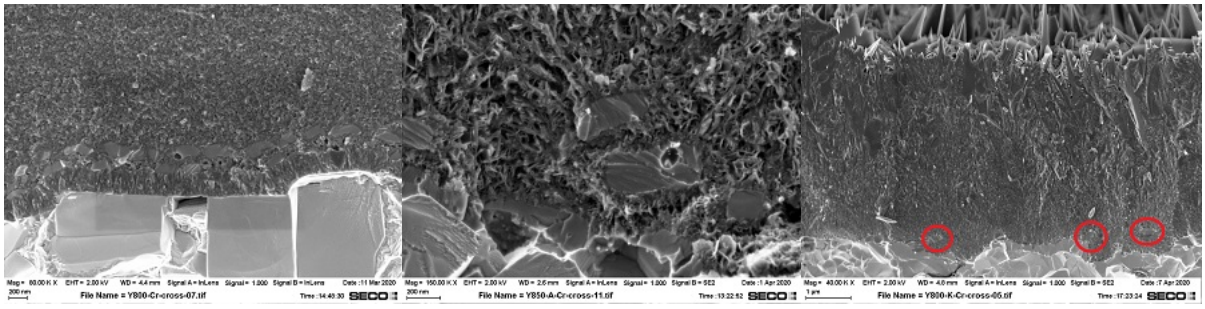

(a) F, Ti(C,O) on chromium. **(b)** P, Ti(C,O) on chromium **(c)** O, Ti(C,O) on chromium, chromium pores in red circles.

Figure 33 Interdiffusion of chromium.

8 Review of MODDE

MODDE is a great tool for visualizing diagrams for more parameter dimensions and mirrors in this respect the reality better. The process mechanisms in CVD are not always linear, growth limiting mechanisms is an example. They are not greatly described by a quadratic formula, especially with a limited set of data points. That said, data points will give you a better and more complex fit and it is important to remember your calculation is never better than your data. In CVD there are many interacting factors and MODDE will help you connect the dots and see connections between responses you would miss otherwise.

In CVD it is often assumed same experiment will yield same result and deviating results are not explained away as outliers. The repetition of experiment D did show, however, the radial thickness and texture coefficient to differ and is an important lesson to keep in mind when analyzing, see Table 4 in Appendix μ.

MODDE will treat all factors equal meaning there is no way of weighing factors during the design of experiments. Due to the nonlinearity of CVD and the limitation of number of experiments, it is hard to extrapolate the result of extreme points in the design space. In retrospect it would have been good to have some more temperature data points due to the expectation that a linear extrapolation between 860°C and 1000°C is a bad fit on the exponential growth rate or morphology.

MODDE may not be optimal for this type of experiments and not all functions were used. The idea is rather simple, optimizing spread of experiments and fit a function to the responses. Image analysis is hard to quantify as a response and this could be a potential area for future machine learning algorithms or Artificial Intelligence that help see connections.

9 Discussion and Conclusion

9.1 Growth planes

The stars in Figure 17 indicates an extremely favorable growth of the {111} twinning boundary and will continuously expose adsorption sites. Larsson et al [21] demonstrate the {111} to be the growth plane in Ti(C,N). The twinning boundary in the Ti(C,N)(<211>) grains are Ti planes and have the most rapid growth rate. Thus is the characteristic flakes of Ti(C,O) probably also centered around a Ti {111} twinning boundary. Ti(C,N) grow <211> grains with an angle of $\sim 55°$ degrees between <100>-sides to <111> (see Figure 3) while Ti(C,O) exhibit a much sharper angle, see Figure 34.

The arms of the star in Figure 34b, 34c and the "feathers" (eg. 36a) for low temperature samples share the feathery feature and displays ultra thin flakes. The thickness of these are in the tens of nanometers, almost flat and the uneven top sides of the flakes might be a few layers of pure Ti and C/O planes. The curvature of flakes and especially feathers are hard to explain and could possibly be due to some non-symmetric charge of the crystal planes.

The Figures 34a, 34d, 34e and 34f demonstrate wider flakes with more clear-cut top sides and a part from the side protrusions, smoother sides. The difference in morphology is telling of another orientation. The wider crystal angle is very sharp and measured to be about 5° degrees between the twinning and side plane and on 34d a small lateral angle can be observed. This could be the reason for the asymmetric protrusions in one end of the flakes. The sharp angles are telling of a very high index plane not observed by XRD. This complicates the use of calculating angles between planes and there are many potential orientations thus characterization requires more advanced methods. High index planes exhibit in general larger surface energy thus being favorable as a bonding layer.

In Figure 34 the types of flake surfaces are demonstrated. Studies on the TiC(111) plane and TiC(001) have been carried out by C. Oshima et al [12]. These show the (111) plane is stable consisting of Ti with similar properties to pure titanium. The TiC(111) plane have a larger surface energy than TiC(001) and show a sticking probability of oxygen two orders of magnitude larger. R. Souda et al [22] show a work function minimizing is achieved by forming Ti(C,O) on the TiC surface by exposing it with O_2. The adsorption sites are demonstrated to be a function of temperature in the range around 1000°C indicating Ti(C,O) crystal formation is a temperature sensitive process.

Due to a large variation of the texture coefficient (see Figure 37 Appendix μ) it is hard to couple process parameters to preferred orientations, similar to that made for Ti(C,N) by von Fiendt [5]. However, sites that will provide more rapid dissociating of the C-O triple bond will be favored during growth. CO having a large dissociating energy means sites with particular strong or/and numerous bonds from surrounding atoms are required to dissociate oxygen. High index planes have a larger surface energy in general and will provide more than one bond-forming possibility and more interaction from the ionic {111} twinning boundary Ti-planes. Thus explaining the high index surface planes.

9.2 Side protrusions

Many of the samples exhibit protrusions or thin facets at the flake side surfaces, these are very rare in the literature. Figure 34a and 34d demonstrate square facets orthogonal to the flake side surface, Johansson [23] describe similar facets on TaC(110), see Figure 35. Both Figure 34a and 34d have protrusions in one end of the flakes, the reason for their difference are likely that the flakes on the fine grained Ti(C,N) are shorter and lacking space to develop. The reason for protrusions only developing in one corner are probably

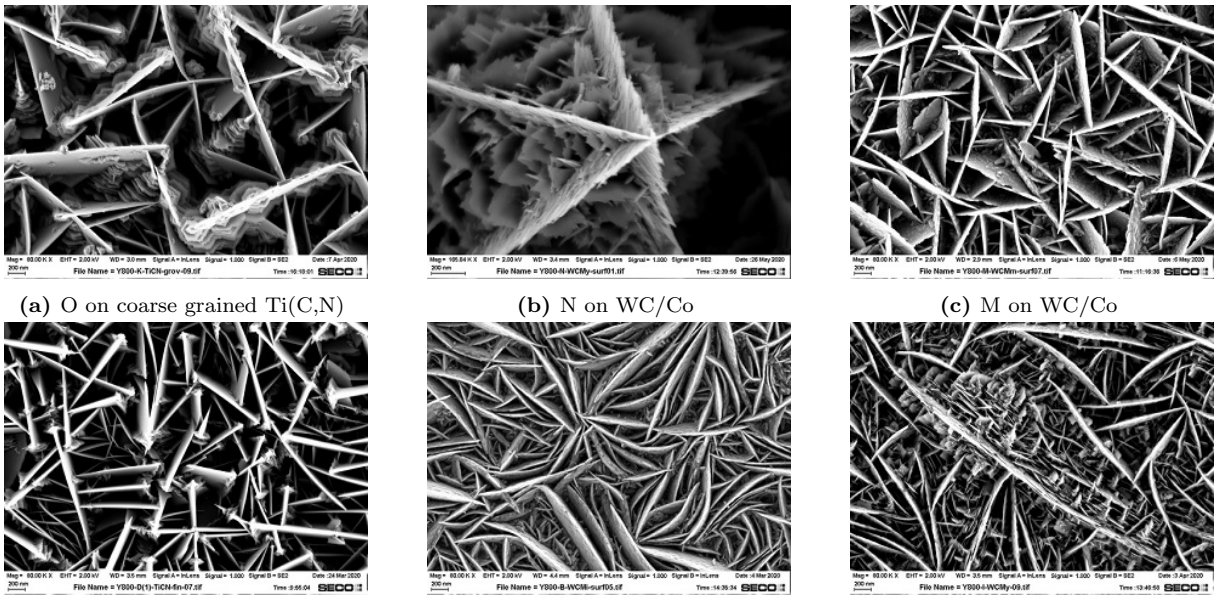

(a) O on coarse grained Ti(C,N) **(b)** N on WC/Co **(c)** M on WC/Co

(d) D(1) on fine grained Ti(C,N) **(e)** B on WC/Co **(f)** I on WC/Co

Figure 34 Different flake morphology of Ti(C,O) coatings.

due to the angle to the twinning boundary, and one side will "open up". The facetes grow 90° to the surface either parallel or horizontal to the growth direction.

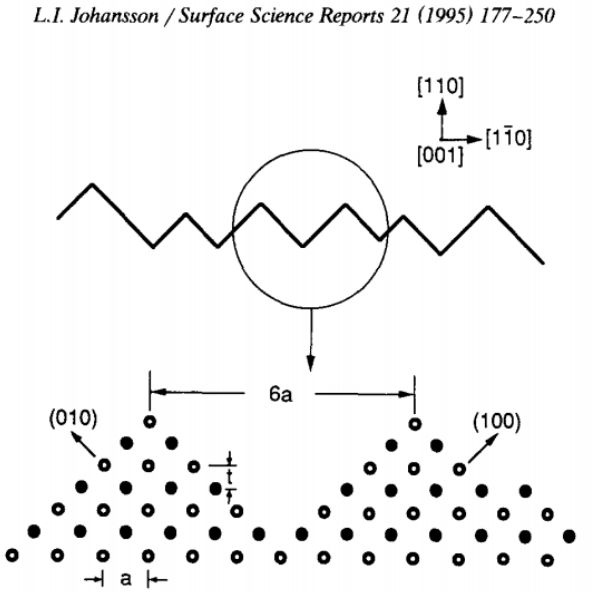

Figure 35 Cross-section profile of alternating (100) and (010) facets for the TaC(110) surface. Facets propagate along the (110) direction with an average periodicity of ~ 6 lattice spacings (From Ref. [23])

Figure 35 demonstrate an example of facets on a transition-metal-carbide, unlike Ti(C,O) these facets are not thin flakes and continue in the [001]-direction (out of the paper). The pervading absence of thick crystals of seemingly all orientations must be attributed to carbon monoxide. If the dissociating energy for oxygen is not large enough oxygen will "block" bonds and further growth. The most extreme facets or protrusions are exhibited by E see Figure 36c indicating a $TiCl_4$ rich environment is favorable for these unknown orientations.

9.3 Stars

A higher ratio of $TiCl_4$ means more stars like K (19b) and high partial pressure of hydrogen leads to more nucleation sites like J (23) contrary to B (17). An abundance of Ti will be able to provide the titanium-heavy twinning boundaries to grow while the hydrogen provides nucleation sites, thus this is a balancing reaction due to nucleation is dependent on titanium, and flake growth is dependent on hydrogen.
Probably then the pentagonal stars in B could be grown with the same abundance as the pine trees in Figure 19b, if the hydrogen was increased in the B-coating. This would create a very different surface than the rest of Ti(C,O) coatings and be similar to the dense coatings of Ti(C,N).

9.4 Growth rate processes

In Figure 21b, the change in activation energy and morphology at a temperature between 930°C and 1000°C suggests change of growth rate limiting mechanism. For the lower temperature morphology the crystals are small and less than 100 nm in length. As the temperature is increased to 930°C they increase to about 200 nm. But general morphology is kept with extremely thin and"feathery" flakes, see Figure 36b. New nucleation sites are preferred over continued crystal growth.

At higher temperature the flakes are allowed to grow larger and the step at the {111} twinning boundary is a preferential adsorption site over new nucleation. The flakes are also wider consisting of a high index plane, see discussion under Surface planes.

Chemisorption of carbon monoxide occurs in a sequential manner. The carbon atom is primarily adsorbed to the surface by molecular chemisorption. If the activation energy is large enough oxygen will dissociate and either leave the surface through desorption or diffuse adsorbing to the surface. Carbon monoxide has the largest dissociation energy for any neutral molecule which would explain the relatively high temperature for growth mechanism transition. This could explain the thin flakes, if the oxygen is not dissociated further crystal growth will be blocked as described in 9.2. In conclusion the high temperature required for dissociation of oxygen contributes to further crystal growth contrary to new nucleation. The rate limiting factor is thus mainly nucleation.

9.5 Nucleation rate dependence on H_2

Increased partial pressure of hydrogen combined with saturation of carbon monoxide yielded the largest growth rate. In Ti(C,N), hydrogen controls the grain size. In Ti(C,O) hydrogen does not have an as direct effect on grain size as it has on nucleation sites and stars. The importance of hydrogen indicates titanium is essential for nucleation, due to the partial reaction $TiCl_4 + 2H_2 \rightarrow Ti + 4HCl$. If the feathers and flakes are centered at {111} twinning planes of titanium then available titanium is essential for nucleation. In sample G, Figure 36a barely any growth occurred in the $TiCl_4$ supersaturated environment but the preference for crystal growth along the twinning planes can be observed. The high deposition rate at low partial pressure of $TiCl_4$ suggests it is never insufficient $TiCl_4$ and the $TiCl_4$+H_2 reaction is reactive while chemisorption of CO is slower.

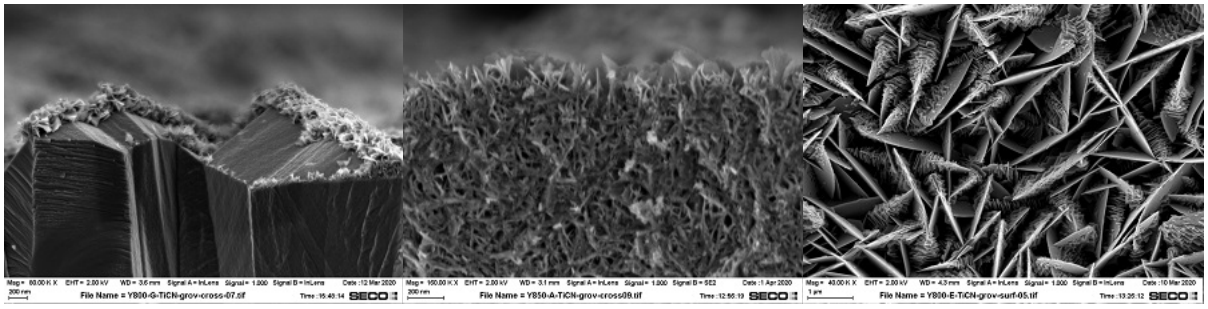

(a) G, coarse grained Ti(C,N) substrate.

(b) P, 160K X magnification. Top most layer on coarse grained Ti(C,N) substrate.

(c) E on coarse grained Ti(C,N).

Figure 36 Varying crystal structure.

9.6 Unit cell and composition

In Figure 30 the lattice parameter dependency on process parameter can be explained by either different C/O composition or more or less vacancies. Vacancies increase exponentially with temperature [15]. Due to no observed change of lattice parameter for increased temperature, this contribution can be considered small or non existent. This indicates also that the ratio of C/O is constant during increased diffusion explained possibly by equal desorption.
Using Vegard's law (Equation 5) and the unit cell for TiC (4.33 Å [12]) and TiO (4.18 Å [24]) the smallest unit cell for the WC/Co samples is 4.27 Å, resulting in $Ti(C_{0.6},O_{0.4})$ while 4.29 Å results in $Ti(C_{0.75},O_{0.25})$ assuming no vacancies.

Compared to the EDS measurements on B; The unit cell yields a composition of $Ti(C_{0.59},O_{0.41})$ by Vegards law while EDS results in $Ti(C_{0.55},O_{0.45})_{0.46}$. Which is a relatively good match, but both results have their own problems and no definite composition can be given.

Increased partial pressure of $TiCl_4$ and decreased CO are the biggest contributors to a larger unit cell thus a larger ratio of carbon to oxygen in the composition. If the carbon atom in the carbon monoxide is the atom primarily adsorbed to the metal and if this process and the process of titanium adsorption is more favorable and quicker than the following oxidization after dissociating of oxygen, it could lead to a larger carbon composition. This could happen at higher pressure of $TiCl_4$ due to Ti exhibiting a quicker adsorption than oxygen making carbon monoxide loose its oxygen atom instead of it diffusing to the most energetically favorable spot, creating a vacancy. Low pressure leads to higher desorption making oxygen leave the surface. While hydrogen makes the titanium more available increasing rate of titanium adsorption.

The samples exhibiting epitaxial crystal growth on Ti(C,N) do have a lattice parameter close to Ti(C,N) at 4.29 Å, see Figure 5. If the coating exhibit about the same lattice parameter as the substrate, strainless crystal growth occur and the coating can continue the epitaxial growth. When Ti(C,O) have a similar lattice parameter as Ti(C,N) the crystals can grow large due to no strain explaining the morphology in eg. Figure 32.

9.7 Flake length

Flake length did not have a good model fit and did not result in any useful information. Had the flake length instead been measured on the coarse grained Ti(C,N) substrates it could be an indication of epitaxial growth on these substrates. Sample I had the longest flakes and the flakes at coarse grained Ti(C,N) seemed longer, but this can be due to topography of the substrate more than to epitaxial growth, see Figure 34f.

9.8 Smoothness

In Figure 29 the increase of $TiCl_4$ in combination of a moderate hydrogen pressure is the largest contribution to even thickness growth. This is probably due to the moderate growth rate. Too rapid growth increase the relative variation of the inherently stochastic process of deposition and a small growth rate increase the risk of sporadic growth and spatial dependency.

9.9 Bonding layer

If Ti(C,O) is to be used as a bonding boundary layer between Ti(C,N) and Al_2O_2, good adhering to the Ti(C,N) is valued and the thinking goes that by exposing a large surface area with high surface energy planes to the Al_2O_2 a good adhering is created. A bonding layer will not be much larger than a couple of hundred nanometers thick. All experiments that shows no sign of a nucleation layer to Ti(C,N) probably have a good adherence, E shows the biggest epitaxial crystals and most side protrusions.

There is a strong coupling between a larger unit cell parameter and epitaxial growth on Ti(C,N). The unit cell for Ti(C,N) is 4.29 Å and a similar lattice parameter for Ti(C,O) will lead to a more strainless crystal growth, as discussed in 9.6. All experiments at 1000°, $TiCl_4/CO \geq 1$ and $H_2 \geq 32$ l/min demonstrate this. The temperature could be lowered to the transition temperature between 930° and 1000° to hinder interdiffusion.

10 Ending words

The process parameters have been correlated to the change of morphology of Ti(C,O) in the perspective of a bonding layer. The path for Ti(C,O) to be the bonding layer for future inserts may be long but this thesis have shined light on an interesting material.

The enormous surface area and the apparent good adhesion to Ti(C,N) is theoretically a perfect bonding layer and the next step will be to put Ti(C,O) to the test. The adhesion to the aluminum oxide top layer needs to be explored and hardness tests has to be carried out.

11 Acknowledgments

I have learned a lot during my time at Seco Tools and the Seco people have been great hosts. My experience at Seco Tools have been a great introductory to what working in research and development in the industry can be like. I could not have asked for a better preparation for a future career, wherever it might take me.

First of all I want to thank Tommy Larsson for taking your time to pedagogically explain and discuss everything from how to use the SEM to crystal orientations and connecting the dots of the result. Filip Lennrick, my supervisor at LTH have constantly been engaged in the work and I really appreciated the opportunity of performing TEM analysis on my samples. Even if the special times have reduced most interactions to online meetings and nothing is normal has Jonas Lauridsen been a great support. Finally I want to thank Dani making the both self and corona inflicted isolation in Fagersta, being far away from home, easier.

References

[1] *Svenska järn- och stålindustrins historia*. May 25, 2020.

[2] Seco Tools AB. 2020-05-12.

[3] Jan-Otto Carlsson. *Handbook of Deposition Technologies for Films and Coatings*. Elsevier, 2010. Chap. Chapter 7 Chemical Vapor Deposition.

[4] P. Carlsson. *Surface Engineering in Sheet Metal Forming, Doctoral thesis*. 2005. ISBN: 91-554-6136-0.

[5] L. von Fieandt. "Cutting Edge Titanium-based CVD Hard Coatings." In: (2018).

[6] R. R. Ford. "Carbon Monoxide Adsorption on the Transition Metals". In: (1970). DOI: 10.1016/S0360-0564(08)60564-7.

[7] *Adsorption Properties of CO on Metal Single-Crystal Surfaces*. June 6, 2020.

[8] S. Ruppi and A. Larsson. "Deposition, microstructure, and properties of nanocrystalline Ti,C,O,N... coatings". In: (2002). DOI: 10.1116/1.1521965.

[9] Hsyi-En Cheng and Min-Hsiung Hon. "Texture formation in titanium nitride films prepared by chemical vapor deposition". In: (1996). DOI: 10.1063/1.362358.

[10] L. Vegard. *Die konstitution der mischkristalle und die raumfüllung der atome, Zeitschrift für Physik. 5 (1): 17–26*. 1921.

[11] W J. Wright D R. Askeland. *Essentials of Materials Science and Engineering, Third edition, SI*. CENGAGE Learning, 2014. ISBN: 978-1-111-57686-8.

[12] S. Zaima Y. Shibata H. Adachi C. Oshima S. Otani M. Aono and Y. Ishizawa. "The surface properties of TiC(001) and TiC(111) surfaces". In: (November–December 1981). DOI: 10.1016/0022-5088(81)90199-5.

[13] F. Lenrick. "Focused Ion Beam Preparation and Transmission Electron Microscopy of Materials for Energy Applications." In: (2016).

[14] K E. Easterling D A. Porter. *Phase transformations in Metals and Alloys, second edition*. Chapman Hall, 1992. ISBN: 978-1-4899-3051-4. DOI: 10.1007/978-1-4899-3051-4.

[15] John J. Hren Albert G. Guy. *Elements of Physical Metallurgy, Third edition*. Addison-Wesley Publishing Company, 1974. ISBN: 0-201-02633-3.

[16] Min-Hsiung Hon Hsyi-En Cheng. "Growth mechanism of star-shaped TiN crystals". In: *Journal of Crystal Growth* 142 (1994).

[17] Duen-Jen CHENG Wen-Pin SUN and Min-Hsiung HON. "Five-ling twinned crystals of titanium carbon nitride". In: *Journal of Crystal Growth* 71 (1985).

[18] Shan Zhou Ming Zhao Tung-Han Yang and Younan Xia. "Decahedral nanocrystals of noble metals: Synthesis, characterization, and applications". In: *Materials Today* 22 (2019).

[19] User Hillbrand at English Wikipedia. *Bragg Diffraction Planes*. May 12, 2020.

[20] B. D. Cullity. *Elements of X-Ray Diffraction*. Addison-Wesley Publishing Company, 1956. ISBN: 0-201-01174-3.

[21] S. Ruppi A. Larsson. "Microstructure and properties of Ti(C,N)coatings produced by moderate temperature chemical vapour deposition". In: (2002). DOI: 10.1016/S0040-6090(01)01712-6.

[22] R. Souda C. Oshima S. Otani M. Aono and Y. Ishizawa. "Structure analysis of oxygen adsorbed TiC(111) by impact collision ion scattering spectroscopy". In: (1988). DOI: 10.1016/0039-6028(88)90404-9.

[23] Leif I. Johansson. "Electronic and structural properties of transition-metal carbide and nitride surfaces". In: (1995). DOI: 10.1016/0167-5729(94)00005-0.

[24] A. David Pearson. "Studies on the lower oxides of titanium". In: (1958). DOI: 10.1016/0022-3697(58)90035-0.

Appendix μ

Table 4 Ratio = $TiCl_4/CO$, t.v.c. = thickness variance coefficient f.g = fine grained, e. g. = evolutionary growth, fth = feathers, fl = flakes, st = stars, b = balls, fl+f = flakes with facets, pt = pine trees.

Name	Ratio	T.°C	P.[mbar]	H_2[l/min]	D.[μm/h]	t.v.c.	Cross	Surf.	**a** Å
A	0.2	860	50	120	0.56	0.028	f. g.	fth	4.285
B	0.2	1000	500	6	0.7	0.41	e. g.	fl, st, b	4.269
C	0.2	1000	50	6	0.62	1.34	e. g.	st, b	4.275
D	1	1000	50	120	0.92	0.098	e. g.	fl+f	4.293
D(1)	1	1000	50	120	1.04	0.0037	e. g.	fl+f	4.294
E	5	1000	500	120	0.91	0.022	e. g.	fl+f	4.293
F	1	860	500	120	0.56	0.013	f. g.	fth	4.282
G	5	860	50	6	0.03	0.05	0	fth	-
H	1	860	500	6	0.08	0.56	f. g.	fth	4.283
I	0.5	1000	500	32	1.11	0.016	e. g.	fl+f	4.275
J	0.2	1000	500	120	2.17	0.098	e. g.	st, pt	4.277
K	1	1000	500	63	1.20	0.068	e. g.	pt	4.282
L	2	1000	500	96	1.03	0.0048	e. g.	pt	4.287
M	3	1000	500	6	0.21	0.035	e. g.	fl+f	4.278
N	1	1000	500	120	1.35	0	e. g.	pt	4.285
O	1	1000	50	63	0.75	0.014	e. g.	fl+f	4.289
P	1	930	500	120	1.40	-	f. g.	fth	4.289

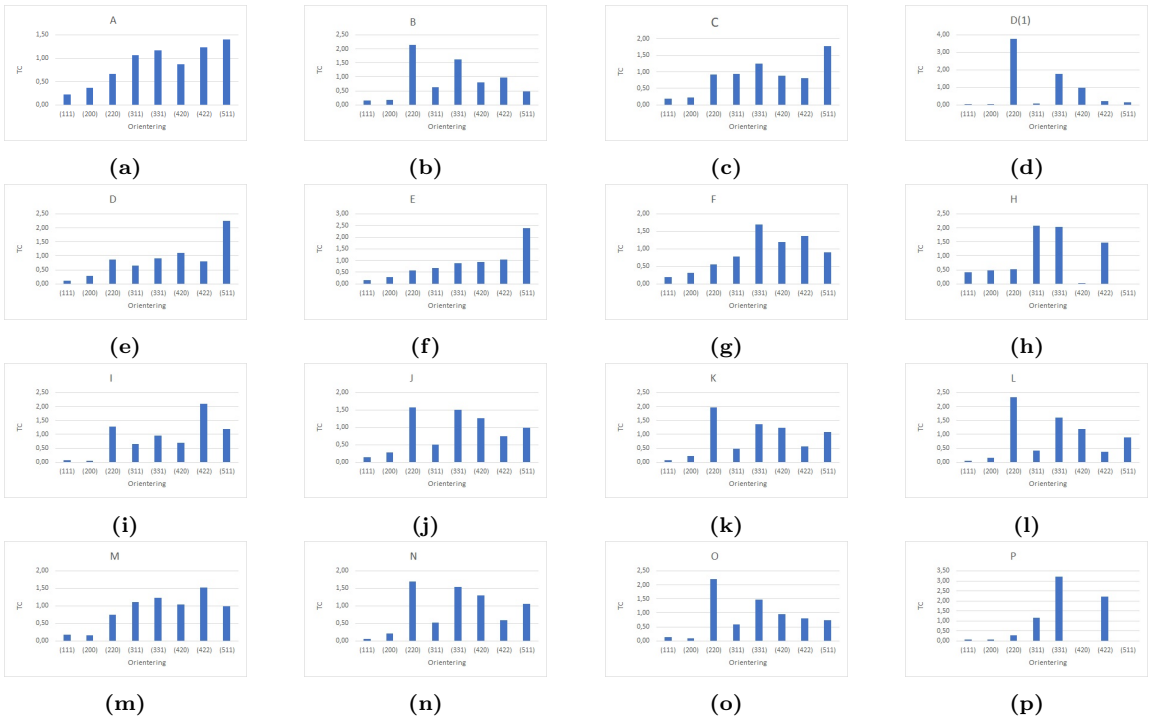

Figure 37 Texture coefficient of all samples on WC/Co. No texture coefficient of G due to no deposition.